The Density of Localized Gap States in Amorphous Silicon-Nitrogen Alloy Films Prepared By Glow Discharge

by

James Frederic White

A thesis
presented to the University of Manitoba
in partial fulfillment of the
requirements for the degree of
Master of Science
in
Electrical Engineering

Winnipeg, Manitoba, 1986

ISBN 0-315-34021-5

THE DENSITY OF LOCALIZED GAP STATES IN AMORPHOUS SILICON-NITROGEN ALLOY FILMS PREPARED BY GLOW DISCHARGE

BY

JAMES FREDERIC WHITE

A thesis submitted to the Faculty of Graduate Studies of the University of Manitoba in partial fulfillment of the requirements of the degree of

MASTER OF SCIENCE

I hereby declare that I am the sole author of this thesis. I authorize the University of Manitoba to lend this thesis to other institutions or individuals for the purpose of scholarly research.

James Frederic White

I further authorize the University of Manitoba to reproduce this thesis by photocopying or by other means, in total or in part, at the request of other institutions or individuals for the purpose of scholarly research.

James Frederic White

The University of Manitoba requires the signatures of all persons using or photocopying this thesis. Please sign below, and give address and date.

ABSTRACT

This thesis deals with the density of localized gap states in amorphous SiN_x:H alloy films prepared by glow discharge. Three different methods are used for the determination: low temperature dark conductivity, space-charge-limited current (SCLC), and the newly-developed modulated photocurrent(MPC). The results show that all three methods give the consistant conclusion that the density of states near the Fermi level is not significantly influenced by the substrate temperature during deposition over the range from 150-400°C. The MPC method also indicates that the density of states is exponentially distributed near the Fermi level.

ACKNOWLEDGMENTS

The author would like to thank Dr. K. C. Kao for his supervision during the course of this thesis.

The author would also like to thank all the members of the MDRL, especially James Schellenberg, Sergio Mejia, and Bob McLeod for assistance and helpful discussions.

CONTENTS

LIST OF FIGURES

LIST OF TABLES

Chapter I

INTRODUCTION

Amorphous silicon has been actively studied worldwide for over fifteen years. Present applications of this material are mainly in xerography and solar energy conversion. With time and thorough research, this material, when incorporated with suitable impuriries, might penetrate the device market. Presently, research is mainly devoted to studying the effect of various deposition parameters on the properties of the material as well as comparing the results of different characterization techniques. So far no deposition procedure is clearly superior, nor has any characterization technique been found to be the best.

When amorphous silicon films are produced, the temperature of the substrate during deposition is one of the key parameters controlling film properties. Important properties of the sample such as dark and photoconductivity are altered substantially over a wide range of this temperature [57]. Since the density of localized gap states is extremely important in determining the transport properties of the samples, it is obvious that the density of states should be related to the substrate temperature during film deposition. The purpose of this thesis is to investigate the existance

of such a relationship. Three experimental techniques are employed for the measurement of the density of gap states near the Fermi level and the distribution of these states in energy.

In this thesis a brief review of previous work related to this thesis topic and some methods for the determination of the density of states that are being used or developed in the Materials and Devices Research Laboratory at the University of Manitoba are given in Chapter II. The three experimental techniques and analysing methods used for the determination of the density of gap states are given in Chapters III, IV, and V, followed by a summary of conclusions in Chapter VI.

Chapter II

REVIEW OF PREVIOUS WORK

This Chapter will review some previous work related to this thesis, particularly the techniques for the determination of the density of gap states, with emphasis on their implementation and their derived results.

2.1 Band Models of Amorphous Semiconductors

An amorphous (non-crystalline) semiconductor is one which has no long-range order in the positioning of its constituent atoms. The most immediate implication of this is that the Bloch theory of transport and the use of the wavevector k are no longer valid. However, short-range order (eg, bonding angles and lengths that are similar to those of the crystalline counterpart), is usually present, which leads to a solid retaining some crystalline-like properties such as the bandgap.

An ideal amorphous solid is considered to be a material that has some degree of short-range order, no dangling (unsatisfied) bonds, and no voids(interior surfaces). These assumptions have led to basically two theoretical models for the distribution of gap states as shown in Figure 2.1 a and b. Because the solid is amorphous, the conduction band mini-

mum and the valence band maximum no longer have sharply defined energies. Instead, the band edges are smeared into tails. The extent of this tailing is the major difference between the Cohen-Fritzsche-Ovshinsky (CFO) [6] and the Davis-Mott (DM) [8] models. According to the CFO model, the conduction and valence band tail states overlap at about mid-gap. The DM model however, assumes a limited amount of tailing (a few tenths of an electron-volt), with an actual energy gap. As well, at the demarcation between the conduction (or valence) band and the tail states, there is a sharp drop in the mobility in the tail states. This drop is associated with localization. The energy difference between these mobility 'edges' defines the mobility or energy gap of the solid. It is obvious that an actual amorphous film will have dangling bonds and other defects present. These imperfections are responsible for the non-zero density of localized gap states being present. Figure 2.1 c shows the density of gap state model assumed to be valid for an actual amorphous silicon film.

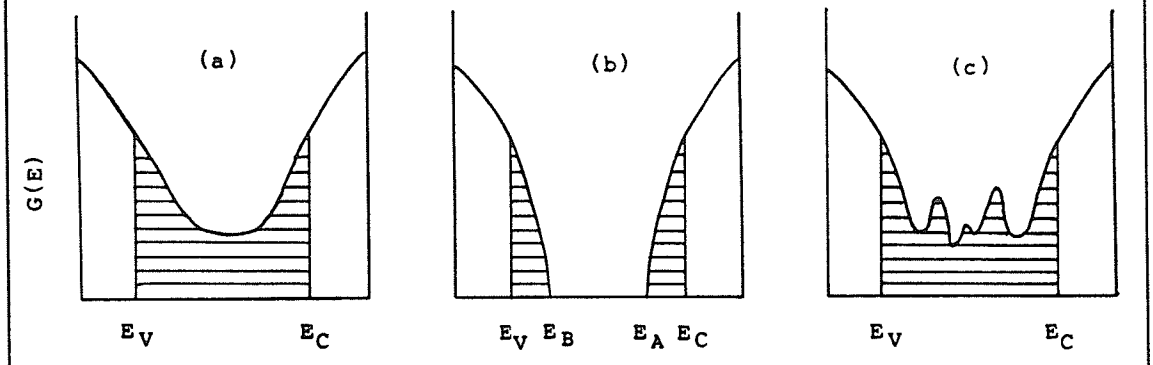

Figure 2.1: Band models for amorphous solids. (a)Cohen-Fritzsche-Ovshinsky model, (b)Davis-Mott model, (c)model for an actual amorphous silicon film. Shaded areas represent localized states.

2.2 Some Properties of a-Si:H and a-SiN_x:H Films

The early work on amorphous silicon was hampered by a large density of gap states. This high density of gap states precluded the use of methods such as the field effect technique for analysis, and the possibility of observing doping effects. However, the introduction of hydrogen into the plasma greatly reduces the concentration of dangling bonds because the dissociated hydrogen can satisfy the valence requirements of the silicon [30], thus reducing the density of states in the gap. The reduction of the density of gap states also enables the observation of doping effects.

The density of states in the gap of a-Si:H films is also dependent on the temperature of the substrates during deposition. Figure 2.2 shows the density of states at the Fermi level measured using a space-charge-limited current technique, as a function of substrate deposition temperature. The density of states is at a minimum of about $5x10^{15}$ $cm^{-3}eV^{-1}$ at a substrate temperature of about 260°C and increases above and below this temperature.

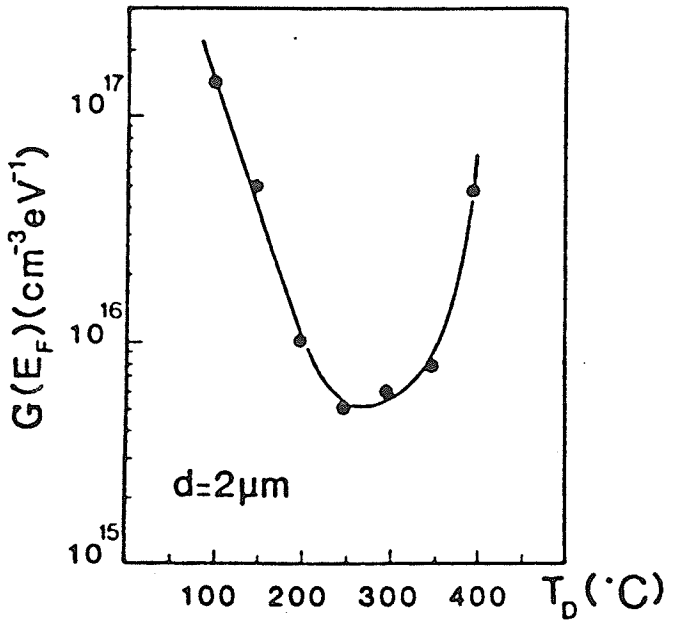

Figure 2.2: Density of gap states at the Fermi level in a-Si:H films as a function of substrate deposition temperature, measured by a space-charge-limited current technique [47].

Staebler and Wronski [51] have reported that there is a change in dark conductivity and photoconductivity of a-Si:H that is a direct result of optical exposure. During exposure to light of wavelength between 6000 and 9000 Å and intensity of 200 mW cm^{-1}, the photoconductivity gradually decreases with time. After the exposure of about two hours has been completed, the observed dark current is smaller than its initial value by almost four orders of magnitude as shown in Figure 2.3. The initial dark conductivity can be recovered if the sample is annealed at a temperature of 200°C for about two hours.

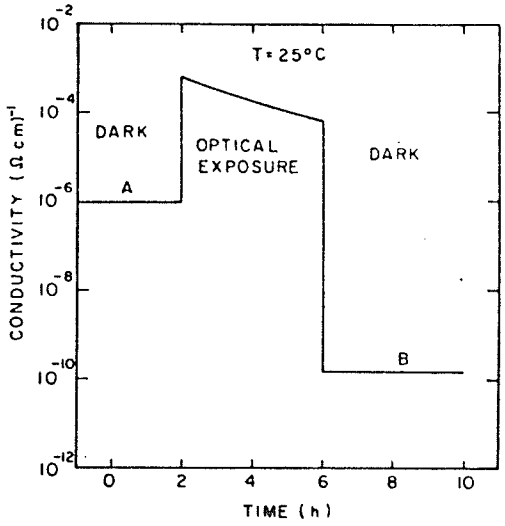

Figure 2.3: Dark conductivity and photoconductivity for a-Si:H films as functions of time, before, during, and after light exposure. Light intensity was approximately 200mW/cm^2 of wavelengths between 6000 and 9000Å [51].

This phenomenon is generally referred to as the Staebler-Wronski effect. The effect is thought to be due to photo-induced defects which create localized states in the energy gap, thus decreasing the conductivity. Jousse et al [21] have reported that using the capacitance-voltage method, the density of gap states of a-Si:H films increases after 30 minutes of exposure to AM1 light. The fatigue effect in photo-luminescence [43] is also thought to be related to the Steabler-Wronski effect, and could be caused by the same mechanism. Because of this effect, any experiments that rely on optical excitation should keep the exposure time to a minimum to avoid any complications.

Nitrogen incorporation in amorphous silicon films is currently experiencing widespread interest. The nitrogen is incorporated in the films produced by the glow discharge of a gas mixture N_2 containing either N_2 or NH_3. Most properties of the films have been found to be dependent on nitrogen content. Kurata et al [24] have reported that the optical bandgap of the amorphous silicon films incorporating nitrogen increases from 1.75 to 5.5 eV as the NH_3/SiH_4 ratio is increased from 0.0 to about 2.2 as shown in Figure 2.4. Also shown in the figure is the ratio of the incorporated nitrogen to the silicon as a function of the NH_3/SiH_4 ratio. Herak et al. [15] have also reported a band gap increase with nitrogen content, but only from 1.55 to 1.75eV; in this case a gas mixture of $N_2+SiH_4+H_2$ was used.

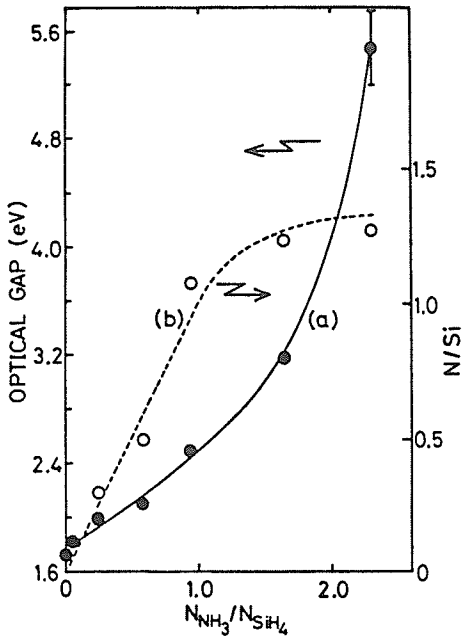

Figure 2.4: Optical bandgap and N/Si ratio of a-SiN_x films as functions of the NH_3/SiH_4 gas mixture ratio [24].

The photoluminescence spectra is shifted to higher energies as nitrogen content is increased [24]. This shift may be attributed to the increase of the optical bandgap due to the nitrogen incorporation.

The dark conductivity of the samples is also dependent on nitrogen content [15] [16] [59]. Using the relation $\sigma=\sigma_1 \exp(E_a/kT)$ to describe the conductivity at room temperature, σ_1 increases with nitrogen content as shown in Figure 2.5. When the nitrogen content x increases past about 0.3, the conductivity drops sharply. This drop is attributed

to the nitrogen being incorporated in the amorphous film as the Si_3N_4 compound, which is a good insulator. The activation energy E_a is almost independent of nitrogen content [15], indicating that the nitrogen is not acting as a dopant since the Fermi level is not shifting.

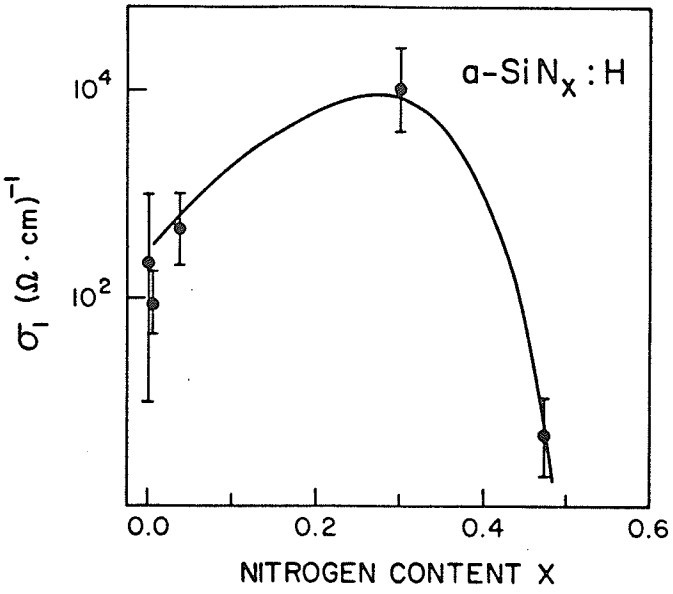

Figure 2.5: Conductivity pre-exponential factor σ_1 as a function of nitrogen content x [15].

Photoconductivity studies by Hirose [16] indicate that the amorphous silicon films incorporated with nitrogen are more stable and exhibit no Staebler-Wronski effect. The photoconductivity however, is quite sensitive to the substrate temperature during deposition [56] as shown in Figure 2.6. As the substrate temperature during deposition is

decreased, the dark conductivity and the photoconductivity decrease also. Below a substrate deposition temperature of 150°C, the photoconductivity becomes negligibly small. Also, as the substrate temperature is increased, less hydrogen is incorporated into the films, and the concentration x of nitrogen decreases slightly from about 0.16 to 0.12.

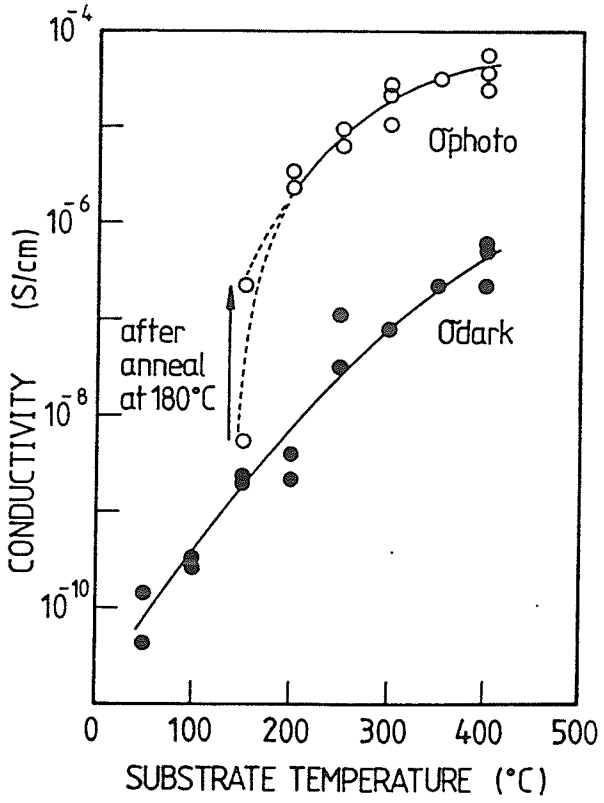

Figure 2.6: Dark conductivity and photoconductivity for a-SiNx:H films as functions of substrate temperature. Photoconductivity measured at a flux of 10^{15} photons per second at 640nm [56].

Doping experiments have also been conducted using diborane and phosphine in conjunction with the silane, nitrogen and/or hydrogen gases [16] [57]. Even with a large amount of nitrogen present, it is still possible to observe the doping effects in the films as shown in Figure 2.7

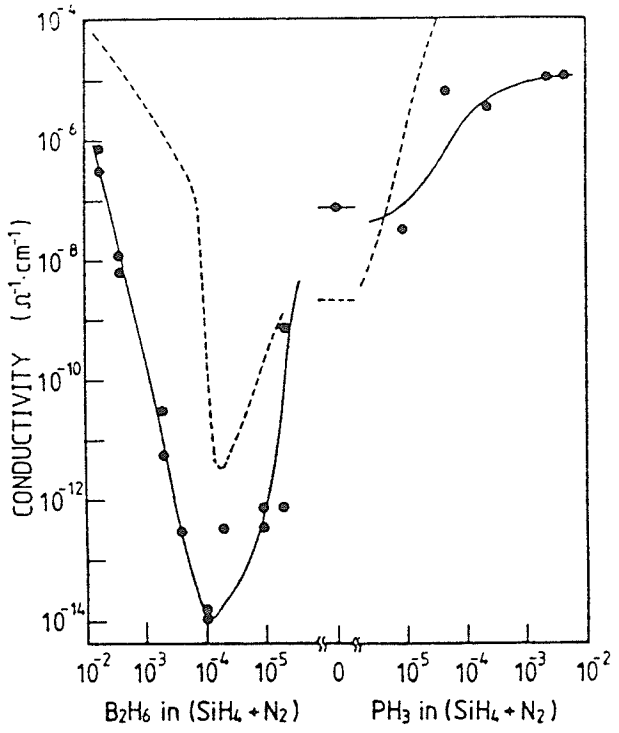

Figure 2.7: The dark conductivity of a-SiN_x:H prepared in B_2H_6 (or PH_3) and SiH_4+N_2 gas mixtures. (The N_2 mole fraction was kept at 50%) [57].Dashed curve is for a-Si:H films from Spear and LeComber [48].

2.3 Determination of the Density of Gap States

A knowledge of the density of localized gap states in amorphous silicon is essential in the characterization of the films. Many experimental techniques such as deep-level-transient-spectroscopy, thermo-power, optically detected magnetic resonance, field effect, space charge limited current, photoluminescence, and the newly developed phase shift analysis of modulated photocurrent have been used for the study of these localized gap states. In this section we shall limit ourselves to the discussion of the techniques which are being used or developed in the Materials and Devices Research Laboratory.

2.3.1 Photoluminescence

Luminescence from amorphous silicon is typically radiated in the near infrared region. The luminescence prefix depends on the method of excitation, ie, thermo-, electro-, or photo-excitation. There have been many published reports on this topic [43] [45] [53], with a more detailed review given by Street [52].

Luminescence is a radiative process competing with nonradiative transitions. If the non-radiative probability is large, luminescence becomes quenched. In Figure 2.8, the luminescent transitions are shown. Band edge luminescence is thought to be the main mechinism for emission and is much stronger than that of the defect band transition. Excited carriers in the conduction band thermalize down to localized

states at the band edge and then radiatively recombine. At low excitation intensities, the recombination is monomolecular and possibly geminate [52]. Defect luminescence occurs when the concentration of carriers at a defect level is large enough so that the probability of recombination becomes significant. Even when defect luminescence is observed, its intensity is still a few orders of magnitude smaller than that of band edge luminescence. Not included in Figure 2.8 are the competing non-radiative transistions which generally include:

- non-radiative tunneling
- thermalization
- deep trapping and subsequent non-radiative recombination
- auger recombination
- surface recombination

which would only serve to decrease the total luminescence intensity.

The film samples for photoluminescence experiments are generally excited using highly absorbed light (usually from an argon laser), and the luminescence is detected with a cooled infrared detector. Amorphous silicon samples only exhibit significant luminescence intensities at temperatures of about 200K and lower. Specialized cooling equipment such as liquid helium or liquid nitrogen cryostats or baths are therefore required. Either the total luminescence signal, a narrow band of the signal, or the spectrally resolved signal

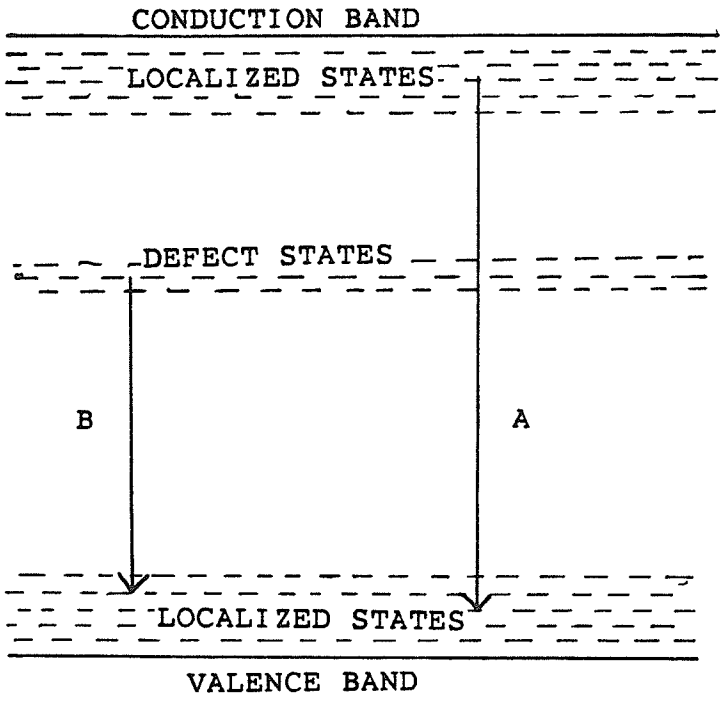

Figure 2.8: Luminescent transitions in a-Si:H. Transition A represents band edge luminescence and transition B represents defect luminescence.

are monitored during the experiment. The following results have been consistently reported for a-Si:H films:

- The intensity of the luminescence signal decreases for increasing temperature for temperatures above about 50K. Below this temperature, the signal remains approximately constant or decreases slightly [50].
- The luminescence signal varies linearly with excitation intensity at low intensity levels, but becomes sublinear as the excitation intensity is increased as shown in Figure 2.9[44].

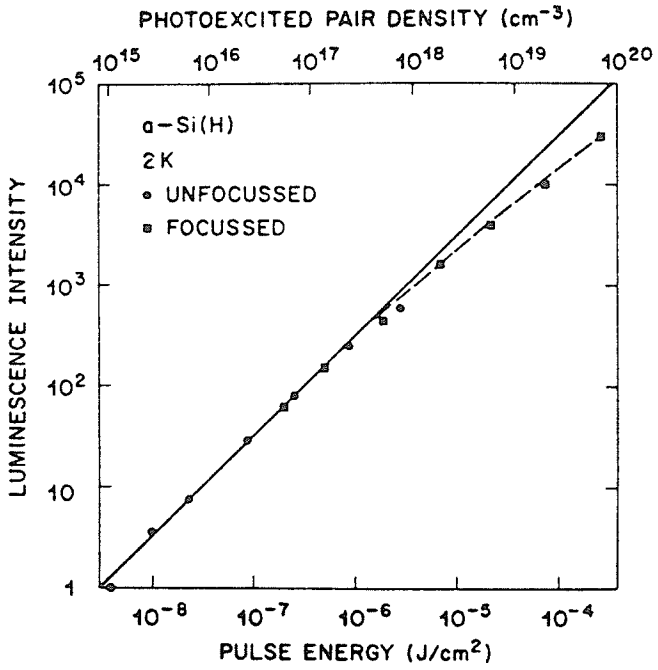

Figure 2.9: Total luminescence intensity as a function of excitation energy. Luminescence was observed at 2K with excitation energy 2.41eV [44].

- The spectrally resolved signal is generally a featureless hump with a peak between 1.25 and 1.4 eV.
- The peak of the spectrally resolved luminescence shifts to a lower energy as the temperature increases. Also, the full width at half maximum increses with temperature as shown in Figure 2.10[39].
- The photoluminescence signal decreases with exposure time. This is the so called fatigue effect which is almost totally reversible after high-temperature annealing and is thought to be related to the Staebler-Wronski effect [55].

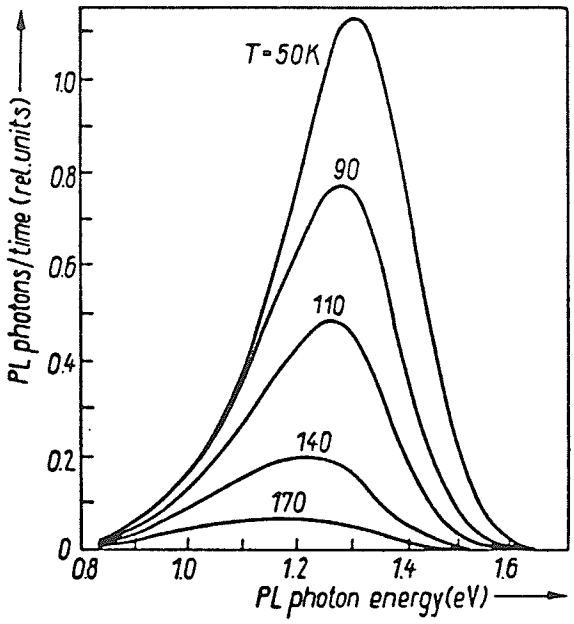

Figure 2.10: Photoluminescence spectra as a function of temperature for an excitation energy of 2.41eV [39].

2.3.2 Thermally Stimulated Currents

Thermally stimulated current (TSC) is another experimental technique which yields information on the density of gap states [10] [22] [27]. The basic experimental arrangement consists of a power supply, a film sample, and an electrometer all connected in series. The sample is cooled in the dark to liquid nitrogen temperatures or less, and then exposed to light for a short period of time. After exposure, the sample is allowed to relax in the dark to reach its equilibrium conditions (ie filled traps) for about fifteen minutes. The temperature is then increased at a constant

rate and the current is then monitored as a function of temperature. As the temperature increases, trapped electrons obtain enough energy to be excited out of their traps, and the current increases. Typical results for a-Si:H films are shown in Figure 2.11.

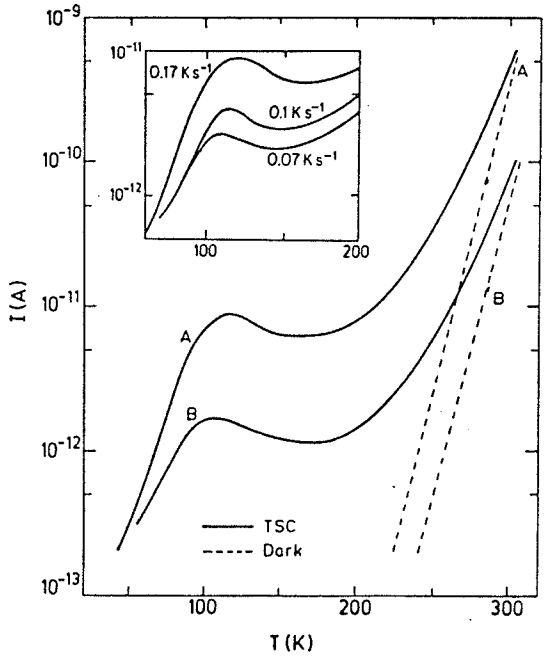

Figure 2.11: Thermally stimulated currents in a-Si:H observed using different heating rates and prolonged optical exposure. TSC exposure time = 30 seconds of red (λ = 670nm) light. Curve A was obtained from a sample previously annealed at 150 °C for two hours. Curve B was obtained from a sample that had been irradiated by a white light for two hours at 300 K [27].

From the temperature Tmax at which a maximum current occurs, it is possible to deduce the position of a dominant trapping level in the energy gap using Equation (2.1) [22].

$$E_c - E_t = kT_{max}\ln(\sigma_1/\sigma_{max}) \qquad (2.1)$$

where σ_1 is the dark conductivity prefactor, and σ_{max} is the conductivity at T_{max}. The major problem with TSC analysis is that the models generally assume a discrete trapping level and not a continuous distribution. This assumption has been criticized by Ibaraki and Fritzsche [19] who have indicated that the maximum in a thermally-stimulated current does not nescessarily correspond to structure in the density of gap states.

It is also interesting to note the reduction of the TSC signal after prolonged exposure to white light in Figure 2.11. Fuhs and Milleville [10] have attributed this reduction to an increase in the density of deep recombination centres in the material. This effect may be related to the Staebler-Wronski effect.

2.3.3 Field Effect

The field effect technique utilizes an electric field to change the conductance of a channel in a structure similar to that of a field effect transistor [12] [14]. If the interface effects are neglected and the semiconductor is assumed to be homogeneous, the current in the channel is given by

$$I(V_F) = (I_0/t)\int_0^d \exp(eV(x)/kt)dx \qquad (2.2)$$

where V_F is the applied transverse voltage, I_0 is the channel current under flat-band conditions, d is the sample thickness, and eV(x) is the amount of band bending as a function of distance x into the sample. By solving Poissons equation

$$d^2V(x)/dx^2 = 4\pi e\rho(x)/\epsilon \qquad (2.3)$$

we can find V(x). In Equation (2.3) ϵ is the dielectric constant of the sample $\rho(x)$ is the filled gap state density which can be written as

$$\rho(x) = \int_{-\infty}^{\infty} G(E)[f(E-eV(x))-f(E)]dE \qquad (2.4)$$

Thus the density of gap states G(E) may be determined from the above equations by initially assuming an arbitrary form for the density of states, and then iteritively modifying the assumed function until all the equations are consistent with each other. Finite temperature statistics should be used in the calculations since the assumption of T=0 can lead to errors as large as 50% when dG(E)/dE is large [12].

Typical field effect data for a-Si:H are given in Figure 2.12. The conductance curves shown are for a sample in a vacuum, after four days, after heat drying, and after illumination as suggested by Staebler and Wronski [51]. After illumination, the sample was annealed at 160°C for several

hours after which the conductance curve of C was again obtained. In Figure 2.13, the density of gap states deduced from each conductance curve of Figure 2.12 is shown.

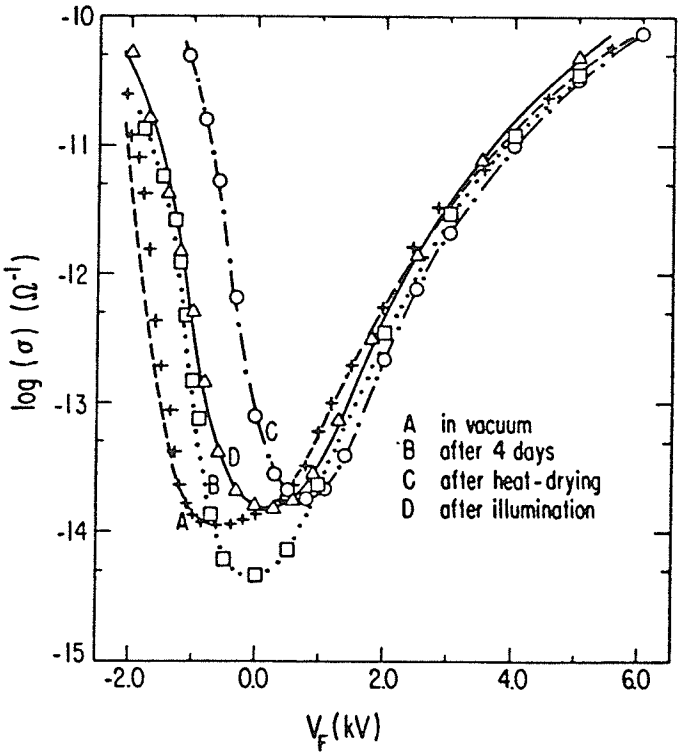

Figure 2.12: Channel conductance of a-Si:H as a function of applied field voltage. The samples were 0.5 μm thick and data were obtained at 60°C in a vacuum. Curve C was obtained after 160°C heat treatment for several hours from the sample that was illuminated [13].

The structure in the density of states in the upper portion of the band gap in Figure 2.13 is possibly non-existent due to experimental error [13]. By assuming the structure-

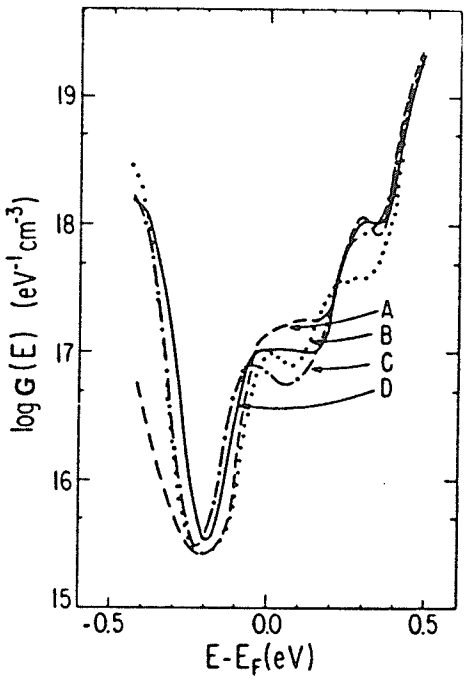

Figure 2.13: Density of gap states calculated from conductance data of Figure 2.12. Curves A, B, C, and D refer to the same conditions in Figure 2.12.

less density of gap states shown in Figure 2.14, Goodman and Fritzsche [13] have calculated the conductance as a function of V_F, and the data are shown in Figure 2.14. It can be seen that the calculated data (smooth curve) are almost coincident with the experimental data of sample D (triangles) from Figure 2.12. Although the two sets of data do not agree exactly, they are certainly within experimental tolerances for almost the entire range of the applied field transverse voltage. This indicates that the field effect results are very sensitive to small differences in the conductance data

and that only the gross characteristics of the gap state profiles should be accepted.

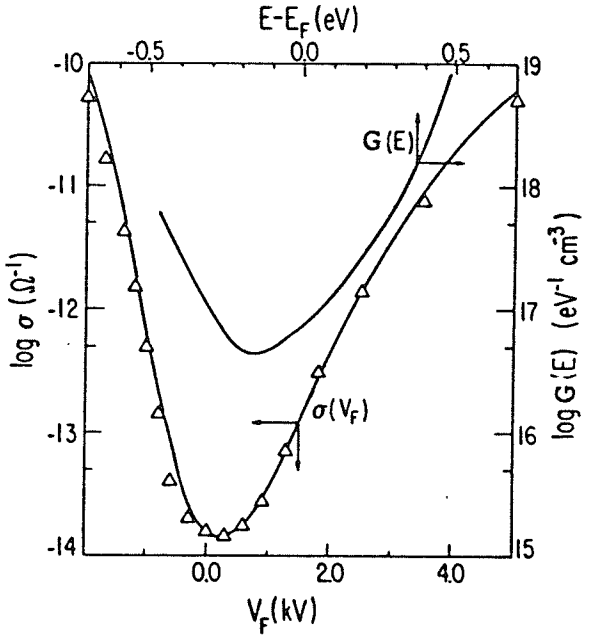

Figure 2.14: Comparison between the experimental conductance data D, and conductance conductance data calculated from the assumed structureless density of states [13].

Another criticism of this technique involves the likeleyhood of only examining the density of states in a region close to the sample surface [12]. If the bulk density of states is significantly different from the surface, the usefullness of this method is obviously limited.

2.3.4 Space-Charge-Limited Current

Space-charge-limited current analysis is used to determine the density of gap states of a-SiN_x:H films in Chapter IV using a method developed by den Boer [9]. This section will review two other methods of analysis developed by Nešpurek and Sworakowski [33], and by Weisfield [58].

The differential method of analysis developed by Nešpurek and Sworakowski uses the slope of a J-V characteristic to determine the density of states in the gap. The working equations used for the determination of the position of the quasi-Fermi level E_{fn} with respect to the conduction band, and the density of states at this level are:

$$E_C - E_{fn} = kT\ln(eN_C\mu_C X_1/t) + kT\ln(V/J) \qquad (2.5)$$

$$G(E_{fn}) = (X_2\epsilon/et^2kT)[V/(m(V)-1)] \qquad (2.6)$$

Where, X_1 and X_2 are the correction factors used to compensate or the non-uniformity of the field (typical values: X_1=1, X_2=0.75 [26]), N_C and μ_C are, respectively, the effective density of states and the drift mobility in the conduction band, V is the applied voltage, J is the resultant current density, and m(V) is dlog(J)/dlog(V) as a function of applied voltage. To analyse the data, a polynomial approximation is made on the log(J) vs log(V) curve. This polynomial is then differentiated and then substituted into Equation (2.6). This method has been compared to that of den Boer [9] by Mackenzie et al [26] who have found that both methods are in agreement to within a factor of two.

Weisfield [58] has claimed to have enhanced the accuracy of the differential method by implicitly accounting for spatial variations of physical properties. In his method, the density of gap states at the quasi-Fermi level and the change of the quasi-Fermi level from Ef can be written as:

$$G(E_f+\Delta E_f) = (Ve/ekTt^2)[\alpha(2-\alpha) + (\gamma-\beta(3-2\alpha)/1-\alpha+\beta/(2-\alpha)] \quad (2.7)$$

$$\Delta E_f = kT\log(J/J\ (2-\alpha)) \quad (2.8)$$

where

$\alpha = d\log(V)/d\log(J)$
$\beta = d^2\log(V)/d^2\log(J)$
$\gamma = d^3\log(V)/d^3\log(J)$
$J_\Omega = \sigma_B V/T$

and σ_B is the bulk ohmic conductivity and is given by $e\mu n_o$, in which n_o is the thermal equilibrium density of free carriers. As with the differential method, a polynomial approximation is used in the analysis of the data. Instead of the factor of two uncertainty in the absolute values for the density associated with the differential method, Weisfield has estimated that the error in his method is approximately 50%. Both methods, however, use the assumption that dG(E)/dE is small. If this is not the case, the error will obviously be larger.

Chapter III

DARK CONDUCTIVITY

One of the basic characteristics of a semiconductor is its conductivity as a function of temperature. This temperature dependence can be used to determine the position of the Fermi level with respect to the conduction band, and also the density of states at this level [32]. Much of the original theoretical work on this topic was done by Mott [29], most of which is still valid today.

3.1 Theory

The dark conductivity of amorphous silicon can theoretically be broken down into three distinct regions [32] given by

$$\sigma = \sigma_1 \exp(-E_1/kT) + \sigma_2 \exp(-E_2/kT) + \sigma_3 \exp(-C_3/T^{1/4}) \quad (3.1)$$

in which the first term on the right-hand-side is due to extended state conduction, the second term is due to band tail conduction, and the third term is due to hopping conduction in localized states at the Fermi level. The derivation of these terms is briefly given below.

3.1.1 Extended State Conduction

A general form for the conductivity of a semiconductor is given by:

$$\sigma = -e\int G(E)\mu(E)kT(\partial f(E)/\partial E)dE \qquad (3.2)$$

where σ is the conductivity, G(E) is the density of states, $\mu(E)$ is the energy dependent mobility, and f(E) is the Fermi distribution function.

Using $\partial f(E)/\partial E = -f(E)[1-f(E)]/kT$, and assuming that the Fermi level is far from the conduction band edge so that the Fermi Dirac function may be approximated by Boltzmann statistics, the conductivity may then be written as

$$\sigma = eG(E_c)kT\mu_0 exp[-(E_c-E_f)/kT] \qquad (3.3)$$

where $G(E_c)$ is the effective density of states at the conduction band edge and μ_0 is the average mobility. This mobility may be examined further along the lines of Cohen [7]. Here, the movement of electrons is considered to be similar to Brownian motion, that is, the mean free path is not greater than the interatomic spacing. Using Einstiens' relation,

$$\mu = eD/kT \qquad (3.4)$$

and writing D in the form

$$D = \gamma a^2/6 \qquad (3.5)$$

We obtain

$$\mu_0 = ea^2\gamma/6kT \qquad (3.6)$$

where γ is the average jump rate and a is the root mean square jump distance. This temperature dependence, along with the pre-exponential factors already in Equation (3.3), give a conductivity of the form;

$$\sigma = \sigma_1 \exp([-(E_C-E_f)/kT] \qquad (3.7)$$

where the pre-exponential factor σ_1 is temperature independent.

3.1.2 Band Tail Conduction

If the atomic wave functions are effectively localized, electronic conduction will proceed via thermally activated hopping. Assuming that a thermally activated mobility takes the form of;

$$\mu' = \mu_0 \exp(-W(E)/kT) \qquad (3.8)$$

and that the tail state profile is distributed as some power s of E,

$$G(E) = G(E_C)(E-E_A)^s/(\Delta E)^s \qquad (3.9)$$

then the hopping conductivity can be written as;

$$\sigma = \sigma_0(kT/\Delta E)^s C \exp[-(E_A-E_f+W/kT] \qquad (3.10)$$

where

$$\sigma_0 = \gamma e^2 R^2 G(E_C)/6 \qquad (3.11)$$

and

$$C = s! - (\Delta E/kT)^{s} \exp(\Delta E/kT)[1+s(kT/\Delta E) + s(s-1)(kT/\Delta E)^{2} + \ldots] \quad (3.12)$$

and $\Delta E = E_C - E_A$ where E_A is an energy defining the lower bound of the conduction band tail state distribution as shown in Figure 2.1.

3.1.3 Fermi Level Conduction

The theory of conduction at the Fermi level, which is similar to impurity conduction, was developed by Mott [29]. The probability of an electron hopping is derived on the basis of the following assumptions:

1. The attempt to escape frequency is less than the maximum phonon frequency ν.
2. The electrons are scattered by phonons between localized energy states separated by an energy W, and these phonons follow Boltzmann statistics so that the probability of finding a phonon with an energy W is $\exp(-W/kT)$.
3. The probability that an electron is transferred between states is given by $\exp(-2\lambda R)$. in which λ is a constant indicative of the wavefunction fall-off and R is the jumping distance.

Thus the jumping probability p can be written as

$$p = \exp(-2\lambda R - W/kT) \quad (3.13)$$

Assuming $D=pR^2/6$ and using Einsteins' relation (3.5), we have

$$\sigma = e^2pR^2G(E_f)/6 \qquad (3.14)$$

Using $G(E_f)/kT$ as the number of electrons that are participating in conduction, and using Equations (3.13) and (3.14), we obtain

$$\sigma = (1/6)e^2R^2\ G(E_f)\exp(-2\lambda R)\exp(-W/kT) \qquad (3.15)$$

At low temperatures hopping is phonon assisted, and the number and energy of the phonons available for these hops is small. For these reasons carriers will not hop to nearest neighbor states, but will hop to states that are closer in energy. The most probable hopping distance can be found by making the exponent in the hopping probability expression a minimum with respect to R. Using N(W) as the density of states per unit volume per unit energy, then the number of states in a sphere of radius R is given by

$$4\pi R^3N(W)W/3$$

Since a hop may occur only if the number of states available to hop to is at least 1,

$$W = 3/4\pi R^3G(E_f) \qquad (3.16)$$

Using this value for W in Equation (3.13), and equating the first derivative of the exponent with respect to R equal to zero, we obtain;

$$R = (9/8\pi\lambda G(E_f)kT)^{1/4} \qquad (3.17)$$

Substitution of Equations (3.16) and (3.17) into Equation (3.15) yields

$$\sigma = \sigma_3(T)\exp-(C_3/T)^{1/4} \qquad (3.18)$$

where

$$\sigma_3(T) = (e^2\nu/2(8\pi)^{1/2})/(G(E_f)/\lambda kT)^{1/2} \qquad (3.19)$$

and

$$C_3 = 18\lambda^3/kN(E_f) \qquad (3.20)$$

Equation (3.18) shows that from the slope of the line on a $T^{1/2}\ln(\sigma)$ vs $1/T^{1/4}$ plot and from an assumed value for λ, the density of states at the Fermi level can be estimated.

3.2 Experimental Details

Amorphous solids can be fabricated by several techniques including sputtering, chemical vapour deposition, electron beam evaporation, and quenching from a melt. For amorphous silicon films, the method most commonly used is the glow discharge decomposition of silane. This method was used for the fabrication of the amorphous silicon-nitrogen alloy films for the present investigation.

The glow discharge decomposition of silane (SiH_4) is the most widely used method for producing hydrogenated amorphous

silicon (a-Si:H) [49] [54]. The procedure involves feeding a gas mixture of silane as well as other gases such as hydrogen, nitrogen, diborane and/or phosphine into a reaction chamber as shown in Figure 3.1. Substrates are placed on the lower plate of the parallel plate configuration, between which a plasma is formed. This plasma is excited by coupling radio-frequency power of 13.56 MHz, to the chamber.

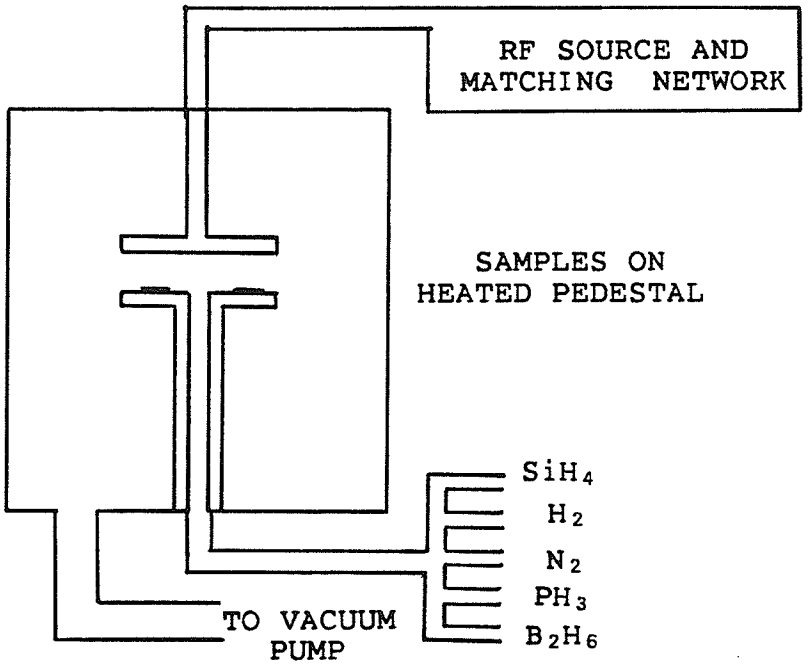

Figure 3.1: Radio-frequency glow discharge system for the fabrication of amorphous silicon films.

It has been found that the properties of the films produced depend on just about all of the deposition parameters

used, such as rf power, substrate temperature, gas flow rate, gas ratios, etc. The samples used here were prepared by the glow discharge of SiH_4-N_2-H_2 gas mixtures and deposited on glass substrates at various substrate temperatures [56] The sample deposition parameters are given in Table 3.1. The concentration of nitrogen x in these a-SiN_x:H films was determined from the intensity of the infrared absorption at 840 cm^{-1}. The concentration was found to be approximately 0.12 and independent of the temperature of the substrate during deposition in the temperature range used here [56] The hydrogen content was calculated similarly and found to decrease from about 15% to about 8% as the substrate temperature during deposition was increased. The thicknesses of the films was measured using a mechanical stylus instrument.

Table 3.1: Deposition Parameters

RF Power Density = 0.1 W/cm^2
Pressure = 2 Torr
N_2/SiH_4 = 0.5

Sample	Substrate Temperature °C	Thickness(μm)
E	150	1.01
F	200	2.24
G	250	1.57
H	300	0.73
J	400	0.89

Planar aluminum gap type electrodes were vacuum-deposited onto the sample surface. The samples were mounted inside a dark cryogenic cooling chamber evacuated to approximately 0.5 Torr. The dark current was measured with a Kiethley 610C electrometer. The temperature of the sample was increased to 330 K and remained there for two hours to drive off any moisture, then it was lowered at a rate of less than 1 degree per minute, during which time dark current measurements were made.

3.3 Results and Discussion

The plot of ln(I) as a function of $1/T$ is shown in Figure 3.2, and the plot of $T^{1/2}\ln(I)$ as a function of $T^{-1/4}$ is shown in Figure 3.3.

The dark currents, instead of the conductivities are used in the presentation of the data for two reasons:

1. The distribution of the current, in the direction perpindicular to the film surface, is probably non-uniform, and this distribution may also vary with film thickness. The sample thicknesses varied by a factor of four.
2. The data required for the analysis are the slopes of the ln(I) vs $1/T$ and $T^{1/2}\ln(I)$ vs $T^{-1/4}$ curves regardless of whether it is the current I or the conductivity σ.

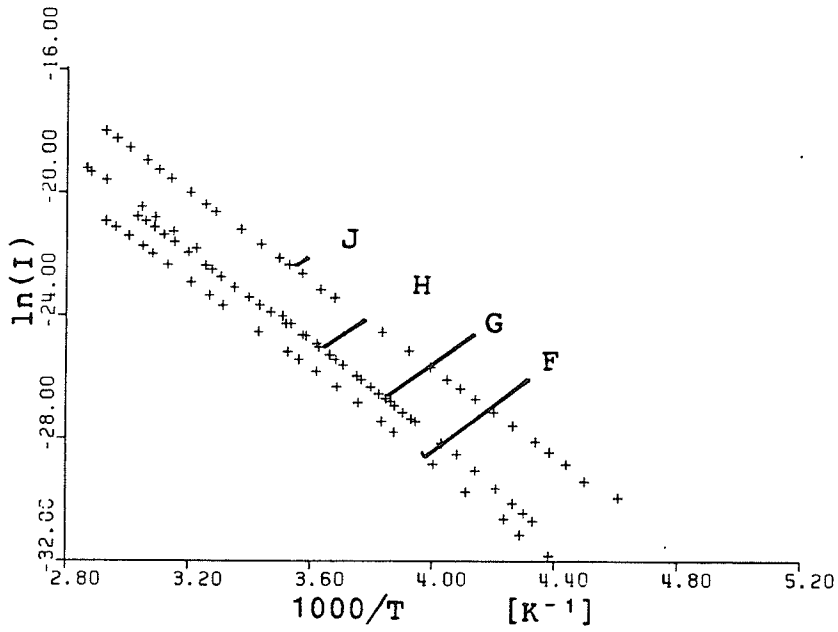

Figure 3.2: ln(I_{dark}) as a function of 1000/T. Substrate deposition temperatures:(F) 200°C, (G) 250°C, (H) 300°C, (J) 400°C.

From Figure 3.2, we have calculated the room temperature activation energy based on Equation (3.7). And from Figure 3.3, we have calculated the density of gap states at the Fermi level based on Equation (3.18). These results are summarized in Table 3.2. For the latter calculation a value of $10^7 cm^{-1}$ was used for λ, corresponding to a 10 Å radius for the localized wave functions [15].

From these results we can conclude that the position of the Fermi level is approximately 0.62 eV below the conduction band edge. This value is relatively independent of substrate deposition temperature in the range from 150 to

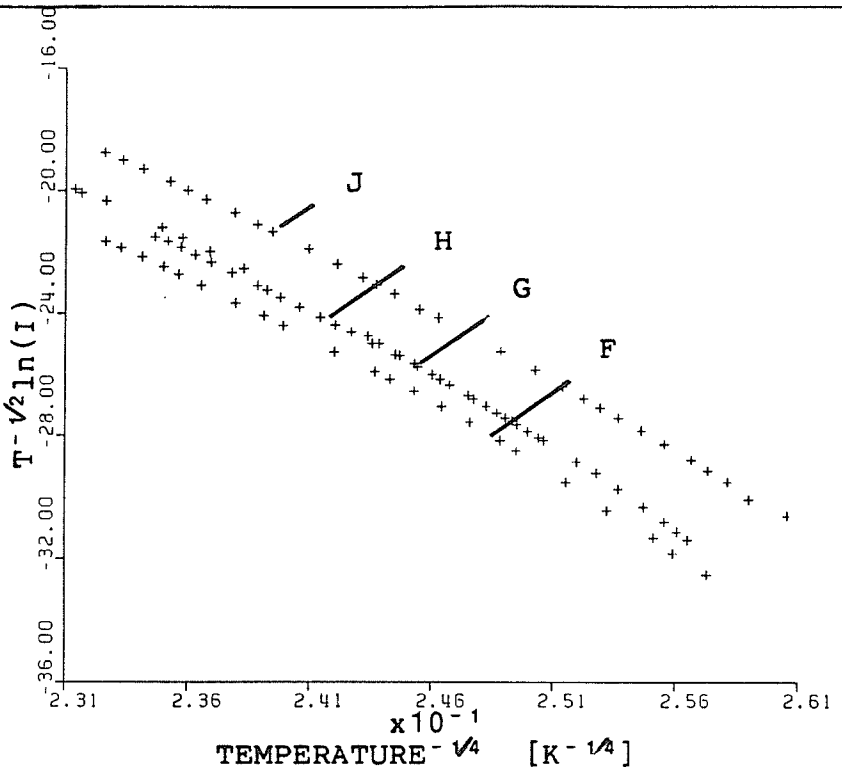

Figure 3.3: $T^{1/2}\ln(I)$ as a function of $T^{-1/4}$. Substrate substrate temperatures:(F) 200°C, (G) 250°C, (H) 300°C, (J) 400°C.

Table 3.2: Activation energy and Density of states at the Fermi level.

Sample	$N(E_f)$ [$cm^{-3}eV^{-1}$]	E_a [eV]
F	$3.0x10^{15}$	0.622
G	$4.4x10^{15}$	0.618
H	$4.4x10^{15}$	0.669
J	$4.6x10^{15}$	0.622

400°C. Also, the density of states at this level is about

$4x10^{15}$ $cm^{-3}eV^{-1}$, which is also independent of substrate deposition temperature in the same temperature range.

Since the conduction current at low temperatures follows a $T^{-1/4}$ dependance quite well, we are therefore confident at least in the relative values of the density of gap states at the Fermi level. Since the actual value of λ is not known, the actual value of the density may differ from the values listed in Table 3.2 by a constant. However, we can say that the density of gap states at the Fermi level, whatever its value, is not significantly affected by the substrate deposition temperature.

Chapter IV

SPACE CHARGE LIMITED CURRENTS

Recently, there has been much work on space charge limited currents (SCLC) in amorphous silicon [9] [11] [26] [47] [58]. The SCLC method has been used for the determination of the density of gap states at the Fermi level, and also the distribution of this density through a finite energy range in the gap.

A classical treatment of the SCLC is given by Lampert and Mark [25]. Generally, the current as a function of voltage follows ohm's law at low fields (ie $I \propto V$), and then enters a space charge limited regime at higher fields. In this regime, the plot of log(I) vs log(V) is characterized by piecewise linear curves.

4.1 Theory

The analysis of the SCLC results to be used here was developed by den Boer [9]. The method consists of calculating discrete shifts in the quasi-Fermi level due to the injected charge, and the associated values for the density of gap states. This method is equivalent to other SCLC analysis methods [26], and is quite simple to apply.

When a voltage is applied to a sample with gap width d, the quasi-Fermi level will shift upwards as the voltage is increased. Also, the density of trapped charge g_t, will shift from its equilibrium value g_{t_0} to g_t accordingly. This shift is mainly due to the increase of the number of filled states. The net increase can be approximately written as

$$g_t - g_{t_0} = \int G(E)dE \qquad (4.1)$$

if the trap density G(E) is continuous and slowly varying. We shall also assume that there is no injected charge gradient and that the electric field is constant and equal to V/d for analytical simplicity. Although contradictory, these last two simplifying assumptions may cause the density of states to be overestimated by not more than a factor of two [25].

Assuming that this gap type structure will behave something like a capacitor and that all the charge is trapped, the injected charge per unit area should be equal to $2\epsilon V/d$. Using Equation (4.1), this gives

$$ed(g_t - g_{t_0}) = 2\epsilon V/d \qquad (4.2)$$

From two discrete points (J_1,V_1), (J_2,V_2) on the J-V curve, the shift in the quasi-Fermi level can be calculated from

$$\Delta E_f = kT\ln(J_2V_1/J_1V_2) \qquad (4.3)$$

From Equations (4.1) and (4.2) we can write

$$2\epsilon\Delta V/d = ed\int G(E)dE \qquad (4.4)$$

This integral can be approximated by $\tilde{G}(E)\Delta V$, where $\tilde{G}(E)$ is the average value of the trap density in the energy range considered by the integral. This result can be combined with Equation (4.4) to give

$$\tilde{G}(E) = 1.5\epsilon\Delta V/ed^2\Delta E_f \qquad (4.5)$$

where 1.5 is used intead of 2.0 as the prefactor in order to give a more realistic value to the density of gap states [26]. Equations (4.3) and (4.5) will then be the working equations for the calculation of the density of states.

4.2 Experimental Details and Results

The sample preparation conditions have been previously described in section 3.2. Planar aluminum gap-type electrodes with various gap widths were vacuum-deposited on the sample surface. Space charge current measurements were made at room temperature in a dark chamber at a vacuum lower than 10^{-4}torr. The currents were measured with a Keithly 610C electrometer. The SCLC measurements were made on samples with gap spacings of about 150μm and 30μm. The results are shown in Figure 4.1 and Figure 4.2.

During the development of the space charge limited current procedure, various samples were used for testing. When

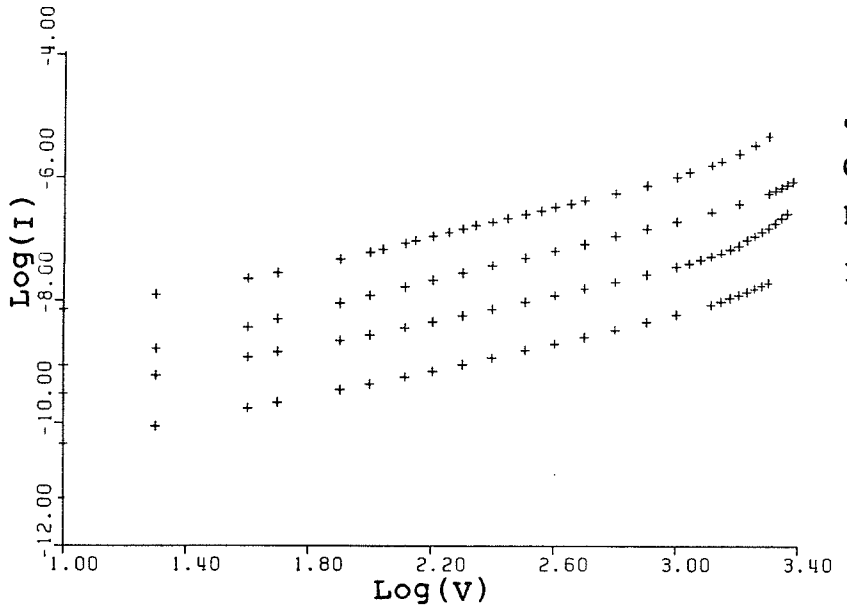

Figure 4.1: Dark current as a function of voltage for gap spacing of 150μm. Substrate deposition temperatures:(F) 200°C, (G) 250°C, (H) 300°C, (J) 400°C.

a sample was used that had a relatively high conductivity, thermal breakdown occurred. Figure 4.3 shows a photograph from an optical microscope that demonstrates this spectacular breakdown. The dark area near the bottom of the picture is the actual sample surface, and is about 180μm across. The straight lines bounding this area are boundaries of the aluminum contacts. As can be seen in some areas, the aluminum was actually removed by the breakdown action. This is most apparent in the breakdown region with a tree-like pattern.

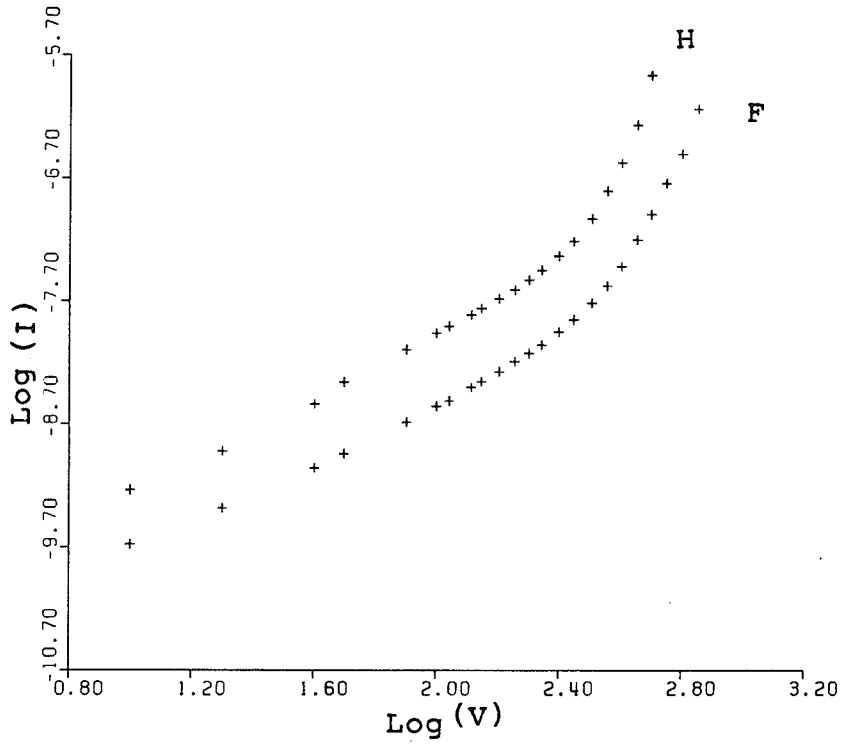

Figure 4.2: Dark current as a function of voltage for gap spacing of 30μm. Substrate deposition temperatures:(F) 200°C, (H) 300°C.

In this particular sample the breakdown occured at about 1100 volts, corresponding to a field of about 6.1×10^4 V/cm, which is quite low, and a power density of about 1000 W/cm^2 flowing across the sample. At power densities such as this it would be expected that sample breakdown would be caused by thermal effects. Figure 4.4 shows the current-voltage relation of this sample. The conduction is ohmic at low voltages but starts to diverge from the ohmic behaviour at about 600V. Just prior to the occurence of breakdown, the

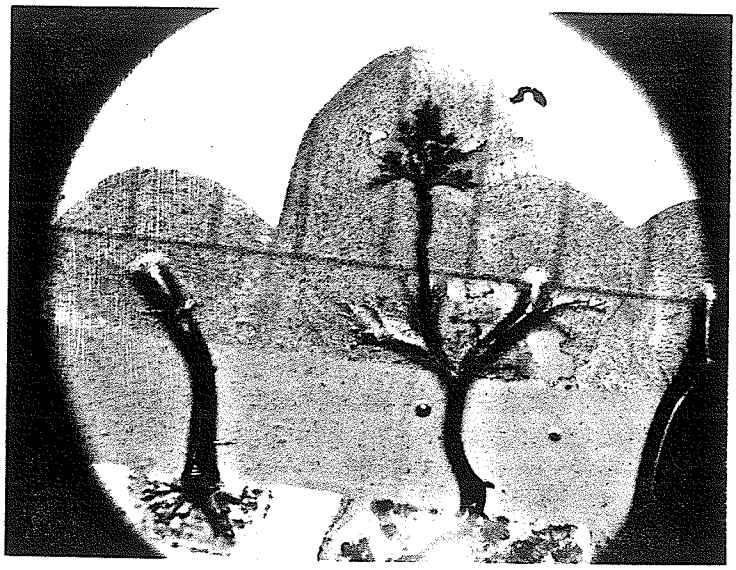

Figure 4.3: Photograph of the sample after breakdown.

current increases rapidly, indicating that heating is leading to final breakdown.

The trunk shown in the far left in Figure 4.3 was further examined under an electron microscope, and is shown in Figure 4.5. This micrograph is focussed on the small dot approximately in the centre of the trunk. Although fuzzy, the photograph clearly shows a hollow tube-like structure running diagonally across the picture. This tube appears to have a crack in it, with a small piece having fallen in. Using X-ray micro-analysis, no significant amount of aluminum was found to be in the structure. Also the scanning

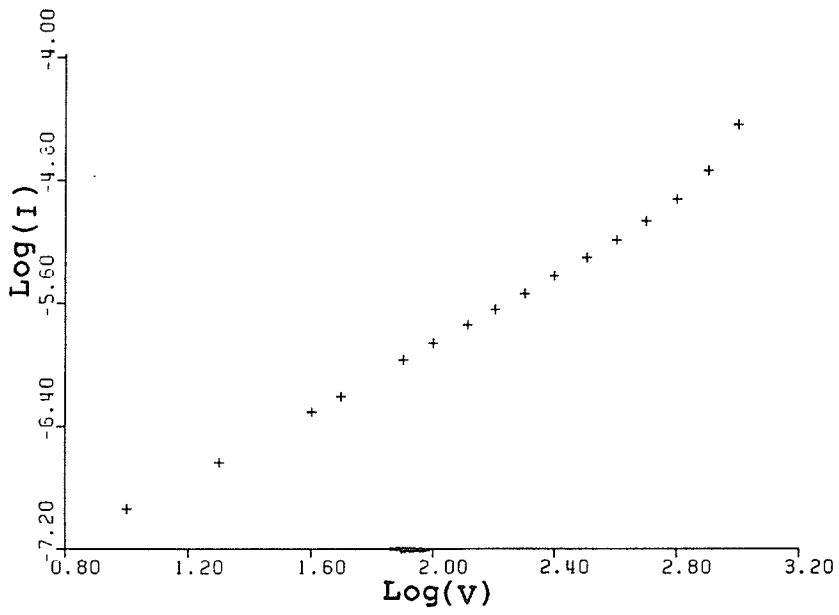

Figure 4.4: Current-voltage characteristic of a-SiNx film.

electron beam was found to charge up the surface, especially around the area of the crack. These observations led to the conclusion that the material of the trunks was indeed silicon.

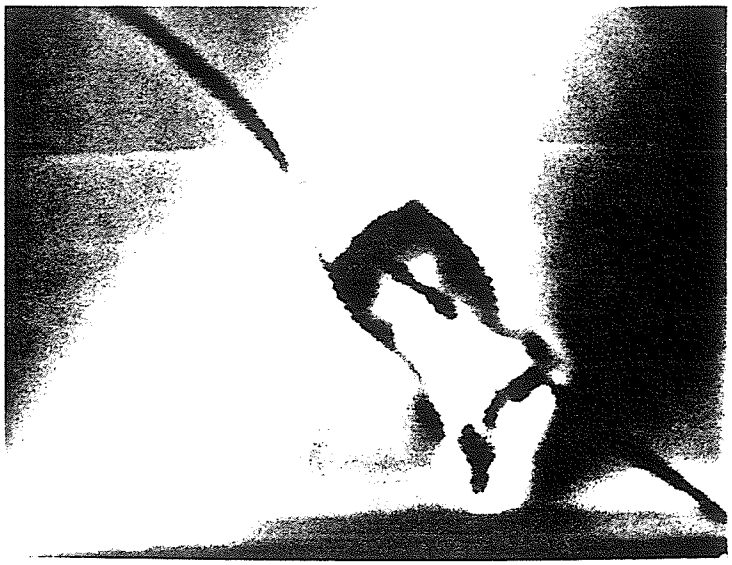

Figure 4.5: Photomicrograph showing the fine structure of the breakdown trunks.

4.3 Discussion

Basically the two electrode configurations for SCLC measurements, which are generally used for counduction current measurements, are the gap and the sandwich cell geometries. The gap cell structure was used here because it was relatively simple to prepare, and also the gap width could be readily changed for scaling law tests. Also, the sandwich cell configuration usually requires dopants to be incorporated into the deposition system to make the contacts ohmic at the low potentials used [40]. Since the gap cell has a much larger gap spacing, the applied potentials can be made

correspondingly larger making the contact potentials unimportant. As well, the samples will not be contaminated by the dopants.

To use the SCLC method for studying the gap state distribution, it is important to ensure that the Poole-Frenkel effect is not influencing the data. Thus the space charge effects will indeed be responsible for the non-ohmic behaviour, and the calculations for the density of gap states will be valid.

4.3.1 Scaling Law

Space charge currents at a constant temperature are given functionally in the form [25]

$$J/d = f(V/d^2) \qquad (4.6)$$

Thus a plot of $Log(I/d)$ vs $Log(V/d^2)$ for samples of varying gap widths d should produce a continuous line in the space charge region. A plot of this form is shown in Figure 4.6 for sample F with gap widths of 30μm and 150μm. As can be seen from the figure, the lines are fairly close to being continuous indicating that the experimental results are following the scaling law.

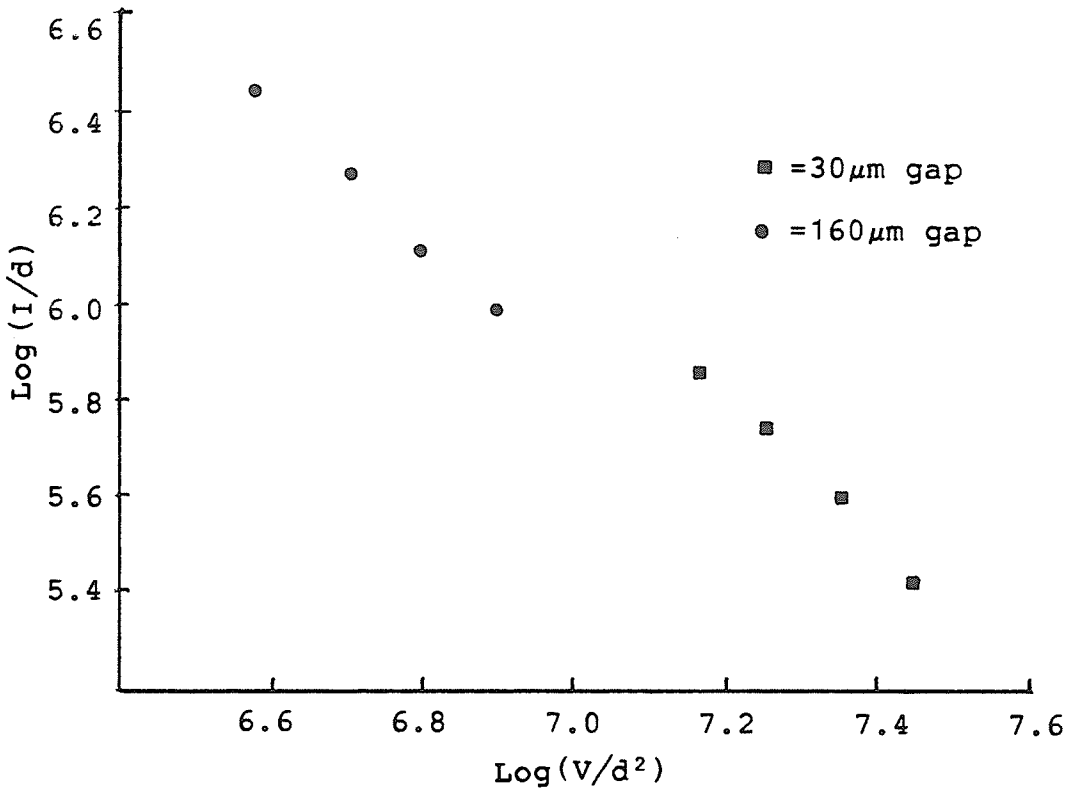

Figure 4.6: The examination of the scaling law for sample F.

4.3.2 Poole-Frenkel Effect

The Poole-Frenkel effect [18] [23] [58] is basically the field ionization of traps that occurs at high electric fields. At fields greater than about 10^5 V/cm, the trap depth is lowered by the field thus enhancing the probability of re-emission of trapped carriers to the conduction band. If this effect is indeed responsible for the non-linear current-voltage characteristic, a plot of log(V/I) vs $V^{1/2}$ will yeild a straight line at high fields [58].

Sample F was used for the examination of this effect, the results are shown in Figure 4.7. It can be seen that the plot is approaching a straight line at higher applied voltages. This indicates that the high field results should not be used for the calculation of the density of gap states.

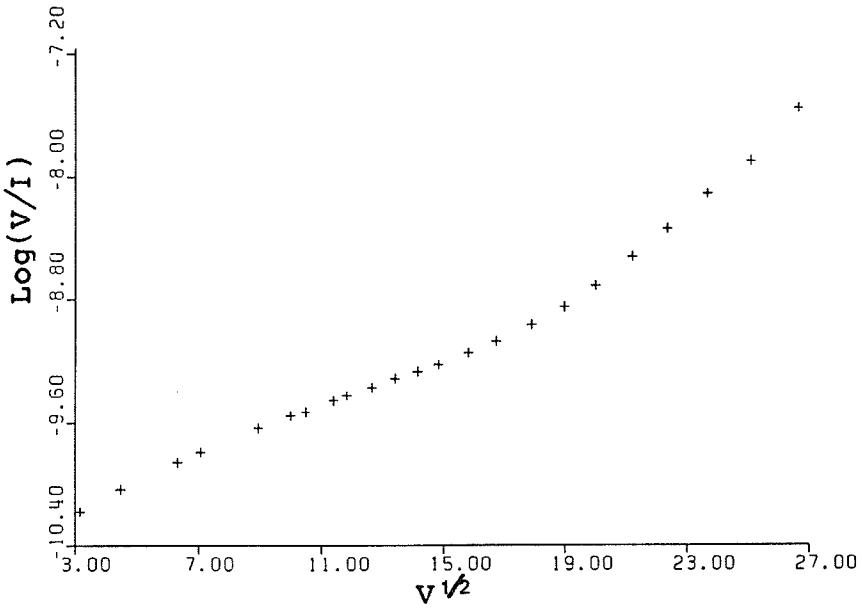

Figure 4.7: The examination of the Poole-Frenkel effect for sample F.

4.3.3 Density of States Calculations

From the preceeding analysis, it appears that our data are indeed in the space charge region at the lower fields. Using Equation (4.3). the shift in the quasi-Fermi level was calculated to be about 0.015 eV (which is approximately at the Fermi-level). Unfortunately, the space charge region

did not extend enough to allow calculation of more than two or three data points. Since a trend for the density of states profiles cannot be depicted from a limited range of data, only the data for the density of states at the Fermi level are presented in Table 4.1. Here, both the data from the wide and narrow gap configurations are shown. The two sets of data agree to within a factor of about 2.

Table 4.1: Density of states at the Fermi-level using SCLC analysis

Sample	$g(E_f)[cm^{-3}eV^{-1}]$	
F	2.3×10^{15}(W)	6.2×10^{15}(N)
G	2.1×10^{15}(W)	
H	2.9×10^{15}(W)	6.0×10^{15}(N)
J	2.8×10^{15}(W)	

(W) refers to the samples with wide gaps and (N) refers to the samples with narrow gaps.

We can conclude that the density of states at the Fermi level is not significantly influenced by the substrate deposition temperature in the range of 200 to 400°C. This conclusion is consistent with that based on the dark conductivity measurements given in Chapter III.

Chapter V

PHASE SHIFT ANALYSIS OF MODULATED PHOTOCURRENT

5.1 Introduction

Recently, a method based on the phase-shift of modulated photo-current as a function of the modulation frequency of the excitation light, has been developed for the determination of the energy distribution of the localized gap states [34]. In contrast to conventional methods such as space-charge limited current (SCLC) [11] [58], field effect(FE) [14] [38], and capacitance-voltage(CV) [16] [46] methods, which utilize steady-state phenomena, this method is based upon a transient phenomenon. The method depends upon the relation between the density of gap states and the phase-shift of the modulated photo-current with respect to the modulated excitation light, at a specific energy corresponding to the modulation frequency.

This method has been used for the determination of the energy distribution of gap states in a-Si:H films by Oheda et al [35], and by Aktas and Skarlotos [1]. Unfortunately, the two sets of results are not consistent with each other as shown in Figure 5.1 and Figure 5.2. However, the results of Oheda et al [35] agree with those of Grünewall et al [14], which, using the field effect technique, show a bump

in the tail state distribution; while the results of Aktas and Skarlotos [1] agree with those of MacKenzie et al [26], which, using an SCLC method, indicate an exponential distribution of gap states. This discrepancy between the results may be due to a legitimate difference in the nature of the gap states because of different fabrication conditions used for these two sets of samples.

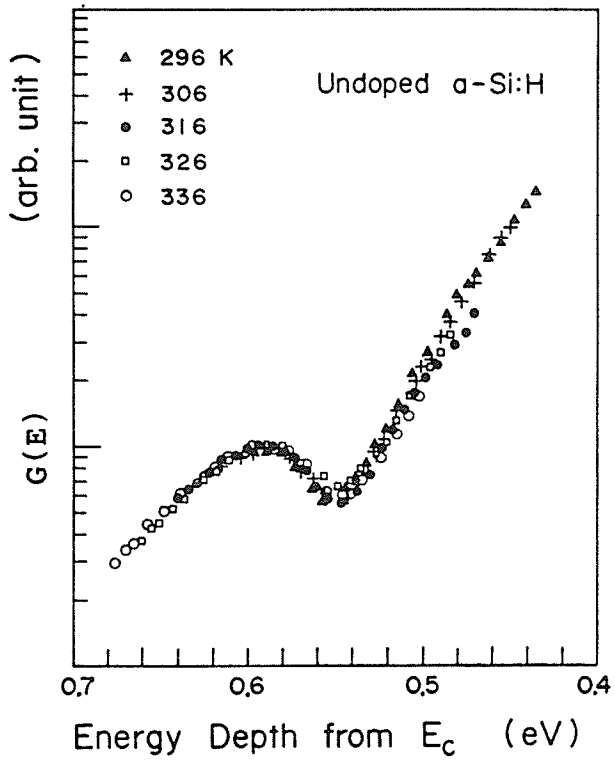

Figure 5.1: Gap state distribution in a-Si:H films according to Oheda et al [35].

In this Chapter we report new results on the gap state distribution profiles in amorphous silicon incorporated with

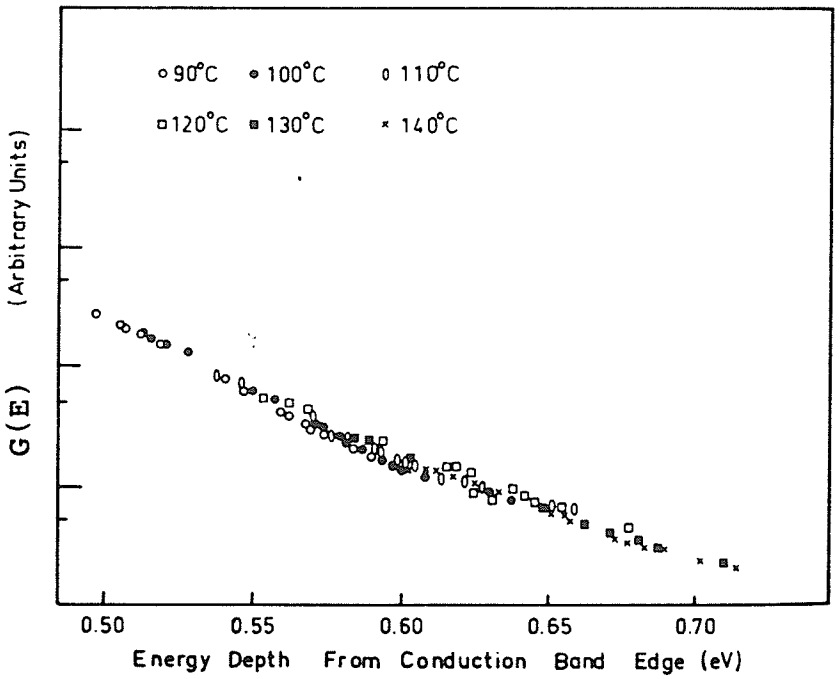

Figure 5.2: Gap state distribution in a-Si:H films according to Aktas and Scarlotos [1].

nitrogen as a function of substrate deposition temperature determined using the phase-shift analysis of the modulated photocurrent.

5.2 Theory

The analysis of the phase shift of the modulated photocurrent is based on the following assumptions:

1. The photocurrent is unipolar.
2. The conduction is trap limited, but proceeds via extended states.

3. The excitation light energy is greater than the band gap.

4. The excitation light intensity varies with time giving rise to a carrier generation rate of

$$g = g_0 + g_1 \exp(i\omega t)$$

with ω the modulation frequency.

5. The capture cross-section of traps is independent of energy.

6. The light intensity is sufficiently low to ensure monomolecular recombination.

The electrons in the conduction band and in traps are governed by the rate equations

$$dn/dt = I_0 + I_1 \exp(i\omega t) - \int_0^{E_d} (dg(E)/dt)dE - (n-n_d)/\tau \quad (5.1)$$

$$dg(E)/dt = n(G(E)-g(E))v\sigma - N_c v\sigma g(E)\exp(-E/kT) \quad (5.2)$$

where n is the density of electrons in the conduction band, n_d is the dark value of n, $g(E)$ is the density of trapped electrons at an energy E below the conduction band, $G(E)$ is the density of states at an energy E below the conduction band, v is the thermal velocity of electrons, σ is the capture cross-section of the traps, and N_c is the effective density of states in the conduction band.

The first two terms on the right hand side of Equation (5.1) represent carrier generation, the third term describes electron trapping, and the last term represents carrier recombination. In Equation (5.2) the terms on the right hand

side represent respectively, the rate of electron capture and the rate of electron re-emission from traps located at an energy E below the conduction band.

The solutions of Equations (5.1) and (5.2) are of the form;

$$n=n_0 + n_1\exp(i\omega t) \tag{5.3}$$

$$g(E) = g_0(E) + g_1\exp(i\omega t) \tag{5.4}$$

Thus n_1, which is related to the density of localized states, can be written as;

$$n_1 = (I_1/(A^2 + B^2)^{1/2})\exp(-i\phi) \tag{5.5}$$

and the relation between the phase shift ϕ and the modulation frequency can be written as

$$\tan(\phi) = B/A \tag{5.6}$$

where A and B can be simplified to [34]

$$A = 1/\tau + \int_{E(\omega)}^{\epsilon_{fn}} v\sigma G(E)dE \tag{5.7}$$

$$B = \omega + \pi kTG(E(\omega)) \tag{5.8}$$

in which

$$E(\omega) = kT\ln(N_C v\sigma/\omega) \tag{5.9}$$

Thus Equation (5.6) gives a relation between the phase shift of the photocurrent, and the density of states at a specific frequency. This frequency is related to the energy $E(\omega)$ through Equation (5.9)

Equation (5.7) can be converted into a summation giving

$$A = 1/\tau_1 + \sum_{s=1}^{j} kT \ln(\omega_s/\omega_{s-1}) v\sigma G(E_{s-1}) \qquad (5.10)$$

where

$$1/\tau_1 = 1/\tau + \int_{E_1}^{E_{fn}} v\sigma G(E)dE \qquad (5.11)$$

In the actual experiment the phase shift ϕ_j and the modulated photo-current I_j are measured as functions of modulation frequency ωj, with j = 1, 2, 3, ... N over a range of temperatures. The suffix j increases as ωj increases. If E_j is not close to the band edge, or $\omega_j \tau_1$ is small enough to be ignored, then the density of gap states from Equations (5.6), (5.8), and (5.10), may be simply written as for j = 1

$$\tau_1 v\sigma G(E_1) = (1/\pi kT)\tan(\phi_1) \qquad (5.12a)$$

and for j = 1, 2, 3, ... N,

$$\tau_1 v\sigma G(E_j) = 1/\pi kT[1+kT\Sigma \ln(\omega_s/\omega_{s-1}) \times \tau_1 v\sigma M(E_{s-1})]\tan\phi \quad (j = 2,3,\ldots,N) \qquad (5.12b)$$

Also, the modulated photocurrent at a modulation frequency ω is theoretically given by

$$I_{ph} = C/(A^2 + B^2)^{1/2}, \qquad (5.13)$$

where C is a constant chosen so that the theoretical magnitude of I_j is normalized to the value of I_1 at ω_1. When this theoretical value of $(I_j)_{calc}$ becomes arbitrarily close to the observed value of $(I_j)_{obs}$, we can consider Equation

(5.12) to be appropriate for the determination of the density of gap states.

5.3 Experimental Details

The fabrication details and film deposition parameters have been described previously in Section 3.2 and are given in Table 3.1.

For the dark and photocurrent measurements, a gap cell configuration with aluminum electrodes was adopted, with an electrode width of 2.0 mm and a separation between electrodes of 1.5 mm. Prior to measurements, the samples were heated to 125°C for about two hours, to drive off any absorbed moisture. The modulated photocurrent was measured at temperatures from 80°C to 120°C using a lock-in amplifier with a reference signal provided by a fast pin diode. The excitation light was from a He-Ne laser whose power was attenuated to a level between 0.1 and 1.0 μW to maintain monomolecular recombination, and chopped mechanically to provide a range of modulation frequencies from 100 to 4000 Hz. Higher modulation frequencies than those used by other investigators [1] [34] [35] were used for this investigation, because it was necessary to ensure that energy levels were closer to the conduction band for valid analysis. The dark current was also measured as a function of temperature using a Kiethley 610C electrometer

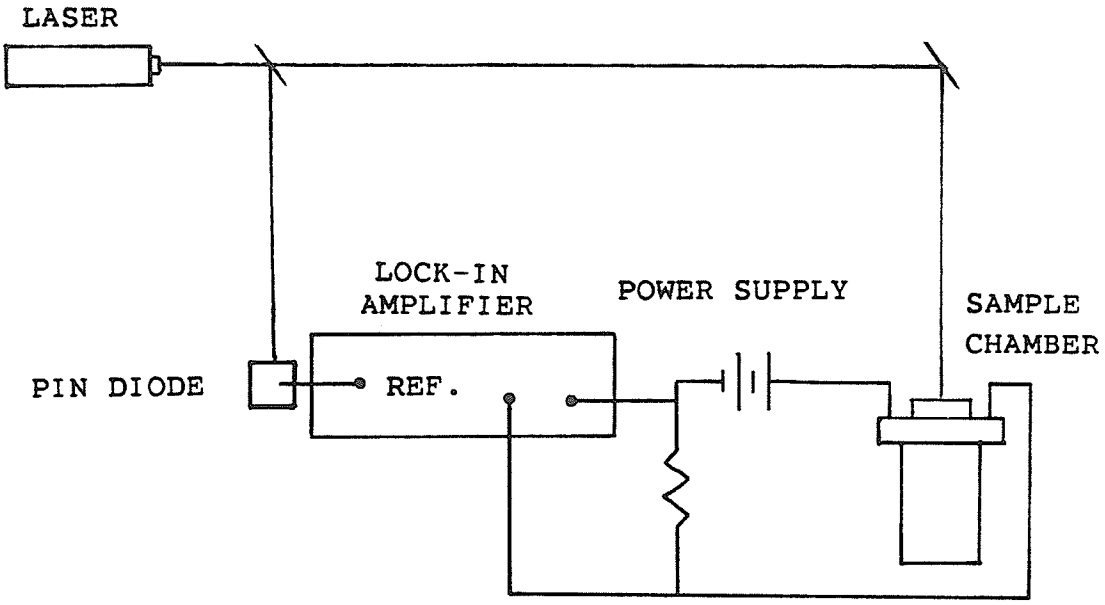

Figure 5.3: Experimental arrangement for the measurements of the phase shift of the modulated photo-current.

5.4 Results and Discussion

From the results of the temperature dependence of the dark current, the activation energy of all samples was found to be between 0.6 and 0.7 eV, which corresponds to the position of the Fermi level below the conduction band edge. This value is consistent with those given in Chapter III. This energy then represents the lowest energy level that can be accurately analyzed in the density of gap states calculations that follow.

Figure 5.4 shows typical results of the phase shift between the exciting light and the corresponding photocur-

rent as a function of modulation frequency, measured at three different temperatures for a sample deposited at a substrate temperature of 400°C.

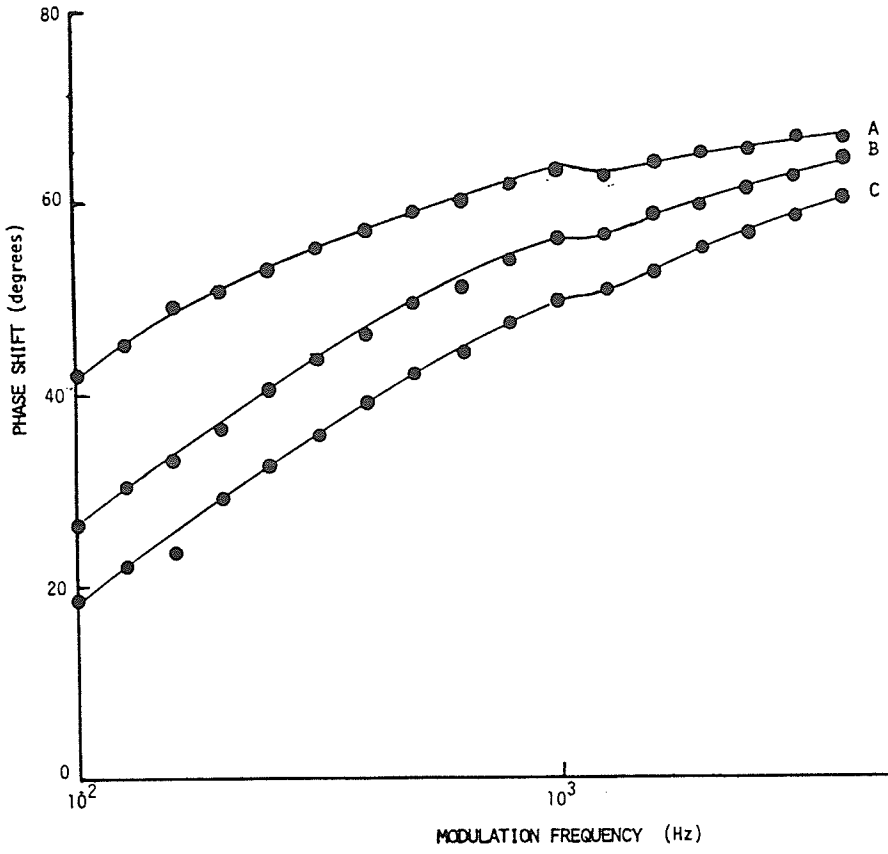

Figure 5.4: The phase shift as a function of modulation frequency of optical excitation. Measured at temperatures of (A) 77°C, (B) 100°C, (C) 112°C, for film deposited at a substrate temperature of 400°C.

The modulated photocurrent magnitude has been calculated as a function of modulation frequency for three different temperatures using Equations (5.6), (5.8), and (5.10) and the measured phase shift. These calculated values, normalized with respect to the first value calculated at 100 Hz, and those measured directly (also normalized to the first value measured at 100 Hz), are plotted as functions of modulation frequency in Figure 5.5. It can be seen that the observed values agree reasonably well with the calculated values. This agreement implies the validity of the method employed for the determination of the gap state distribution profiles. However, it should be mentioned that at temperatures outside the range of 80°C to 120°C, there is a discrepancy between the calculated and the observed values of the modulated photocurrent.

The relative density of gap states, $\tau_1 v\sigma G(E)$ as a function of modulation frequency, calculated from equations (5.12), is shown in Figure 5.6. For this calculation the product $N_c v\sigma$ is assumed to be independent of temperature. Since the temperature dependence of the optical gap in the temperature range used is negligibly small, the temperature dependence of the density of gap states is due almost entirely to the temperature dependence of E_j [1]. According to Equation (5.9), $E(\omega)$ is proportional to temperature for a fixed ω. Thus the frequency scale for the spectra shown in Figure 5.6 can be converted to an enegy scale. Using a value

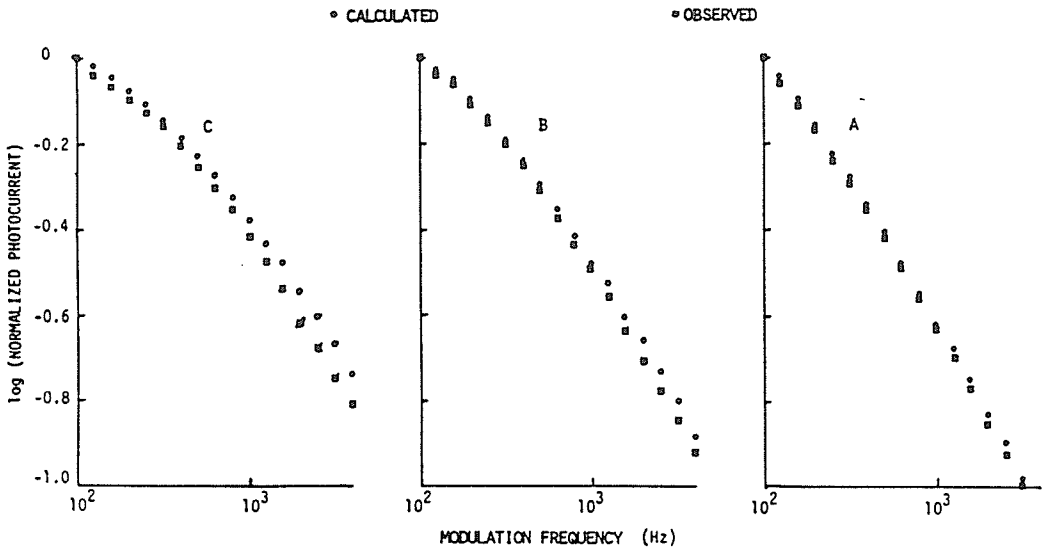

Figure 5.5: Normalized values of the calculated and observed photocurrent as functions of modulation frequency. Measured at temperatures of (A) 77°C, (B) 100°C, (C) 112°C, for film deposited at a substrate temperature of 400°C.

of 10^{11} for the attempt to escape frequency ($N_c v\sigma$), we have calculated the relative density of gap states as a function of energy and the results are shown in Figure 5.7. There are some overlapping regions of gap states due to different temperature-frequency combinations corresponding to the same energy. Clearly Figure 5.7 indicates that the density of gap states is exponentially distributed in the gap. A similar result for amorphous silicon-nitrogen alloy films measured by an SCLC technique has been reported by Furakawa et al [11]. A least mean squares approximation, fitted on the

data in Figure 5.7 gives a slope of -8.5 with a correlation coefficient of -0.995.

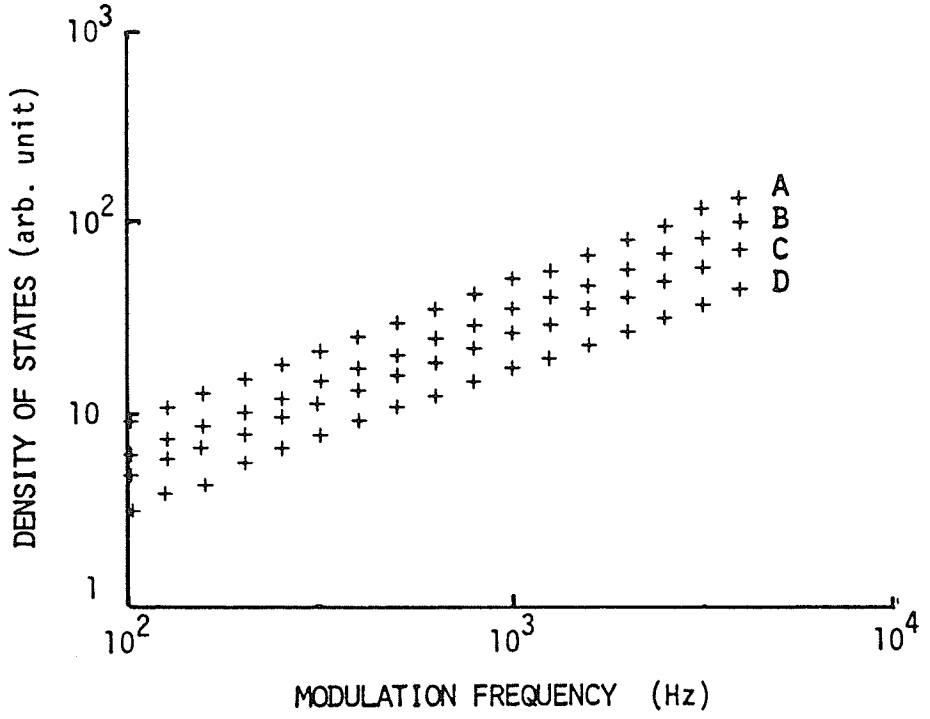

Figure 5.6: The relative density of gap states as a function of modulation frequency. Calculated from measurements at (A) 77°C, (B) 92°C, (C) 100°C, (D) 112°C, for film deposited at a substrate temperature of 400°C.

Following the same procedure, the gap state distribution profiles for all the samples listed in Table 3.1 have been determined, and the results are shown in Figure 5.8.
All the samples exhibit an exponential distribution, at least in the energy range from 0.45 eV to 0.65 eV below the

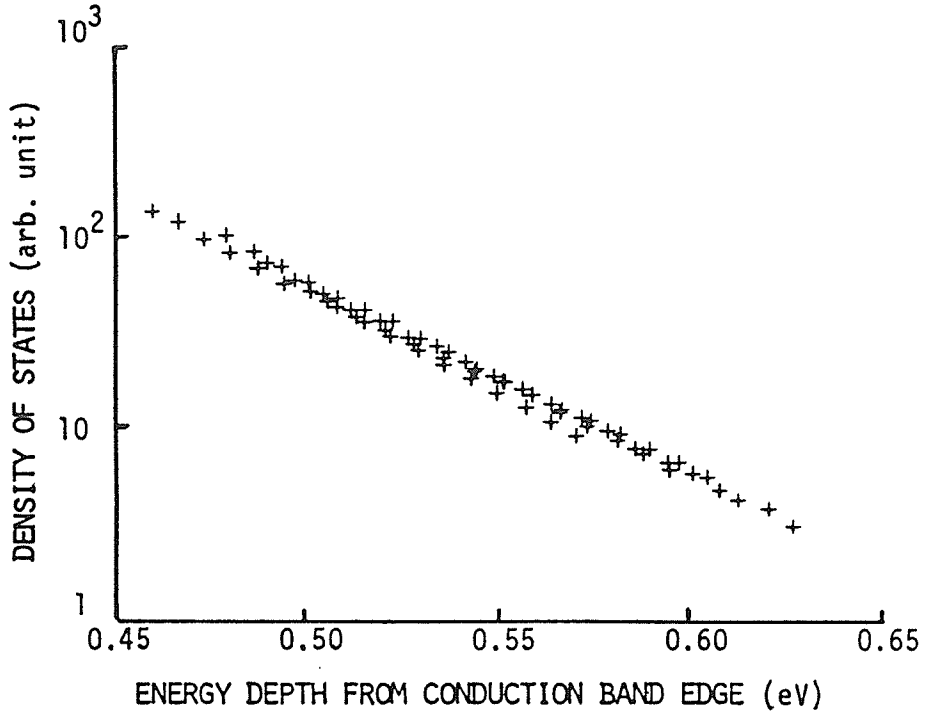

Figure 5.7: The relative density of gap states as a function of energy for the film deposited at a substrate temperature of 400°C.

conduction band edge. The slopes of the lines are all between -8.5 and -9.7, and all have correlation coefficients between -0.992 and -0.997. Assuming an exponential trap distribution of the form

$$G(E) = (N_t/kT_t)\exp[-(E_c-E)/kT_t] \qquad (5.14)$$

where N_t is a trap concentration parameter, E_c is the conduction band edge, and T_t is the characteristic temperature of the distribution. We have calculated T_t from the data in Figure 5.8, and the values of T_t for all the samples under

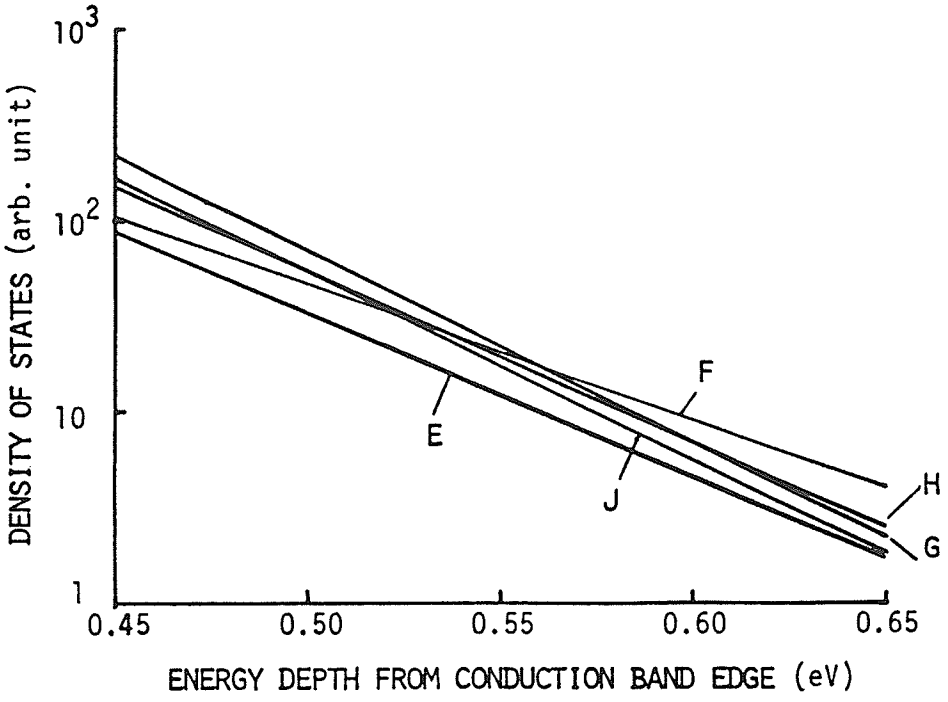

Figure 5.8: The relative density of gap states as a function of energy for films deposited at various substrate temperatures. (E) 150°C, (F) 200°C, (G) 250°C, (H) 300°C, (J) 400°C.

investigation are between 440°K and 502°K, in reasonable agreement with those reported by other investigators [11].

On the basis of the above results, the substrate temperature does not appear to affect either the gap state distribution profile or the characteristic temperature, at least in the energy range around the Fermi level. Since the parameters τ_1, σ, ν and N_c are not known, it is not possible to obtain the absolute value of G(E) by this method. However the results from chapters III and IV indicate a gap state

density of about $4x10^{15}$ $cm^{-3}eV^{-1}$ at the Fermi level, and this value is independent of substrate deposition temperature. This implies that the changes in electronic and optical properties resulting from a change in the substrate deposition temperature [15] [57] can be attributed to the change in the density of gap states at energy levels far away from the Fermi level.

Our results differ from those of Solomon et al [47], who have reported that for a-Si:H films, the density of states at the Fermi level, depends on the substrate deposition temperature, and reaches a minimum at about 260°C as shown in Figure 2.2. Their results are quite different from ours for a-SiN_x:H films. It is possible that the nitrogen incorporated into the films tends to reduce the density of states at the Fermi level over a wider substrate deposition temperature range.

Figure 5.6, does not show any structure in the density of states. When present, this structure can be used to calculate the attempt to escape frequency. Figure 5.9 shows the G(E) vs frequency relation as obtained by Oheda [35]. The arrows in the figure indicate the relative maxima of the curves, and all correspond to the same energy. By plotting the frequency at which the peak value of G(E) occurs as a function of inverse temperature, we can calculate this energy. Using this energy and Equation (5.9), we can then calculate the attempt to escape frequency.

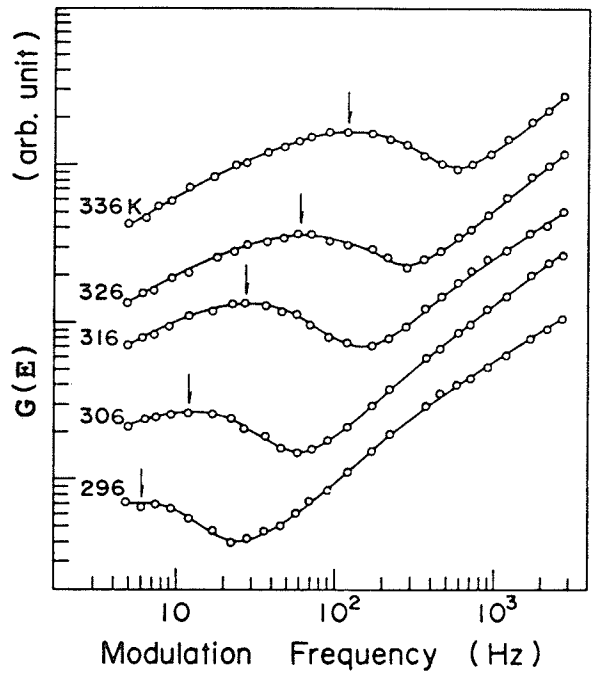

Figure 5.9: Density of gap states vs frequncy relation obtained by [35]. Arrows on figure indicate frequency-temperature combinations corresponding to identical energies.

We can conclude that the gap state density distribution profiles for nitrogen incorporated amorphous silicon films is exponential in energy, and independent of substrate deposition temperature at least up to 0.2 eV above the Fermi level. The present method, based on the phase shift analysis of the modulated photo current, gives reasonable results for the distribution profiles. However, it would seem nescessary to justify the assumption that the energy dependence of the capture cross-section is not appreciably influencing the results.

Chapter VI

CONCLUSIONS

The density of states profiles for amorphous silicon-nitrogen alloy films has been measured using three methods, temperature dependance of dark conductivity, space-charge-limited currents, and phase-shift analysis of modulated photo-current. The results from all three methods indicate that the density of gap states, and the distribution profiles near the Fermi level are not significantly affected by the substrate temperature during deposition in the range from 150 to 400°C. The first two methods are in good agreement with each other as to the density of states at the Fermi level, which is of the order of 4×10^{15} $cm^{-3}eV^{-1}$.

Since the density of gap states and their distribution profiles near the Fermi level are independent of the substrate deposition temperature, the cause of the dependence of the electrical and optical properties of amorphous silicon incorporated with nitrogen on the substrate deposition temperature is most likely due to the change of the density of the gap states closer to the conduction band. This hypothesis however, must be confirmed by another technique such as the field effect method which is able to monitor a larger energy range in the gap.

APPENDIX A

The computer program used to analyse the experimental data in Chapter V is as follows:

```
//    JOB ',,I=10'
/*MAIL PLEASE DO NOT STAPLE ME
//S1 EXEC FORTXCLG,USERLIB='SYS4.DRIVER.XEROX'
//FORT.SYSIN DD *
C
C
C
C       WRITTEN AND DIRECTED BY JAMES WHITE
C
C THIS PROGRAM WILL ANALYSE DATA ACCORDING TO THE
C ALGORITHM BY H. OHEDA (J. APPL. PHS. 52(11) 6693).
C DATA IS ENTERED IN FREE FORMAT AS FOLLOWS:
C
C           ATTEMPT TO ESCAPE FREQUENCY
C           NUMBER OF DIFFERENT TEMPERATURES
C           TEMPERATURE 1
C           NUMBER OF DATA PAIRS
C           FREQ1 PHASE1
C           FREQ2 PHASE2
C           ETC
C           TEMPERATURE 2
C           NUMBER OF DATA PAIRS
C           FREQ1 PHASE1
C           ETC
C
C      THE OUTPUT DATA GIVES THE THEORETICAL VALUE OF
C PHOTO-CURRENT TO BE EXPECTED, AS WELL AS THE RELATIVE
C DENSITY OF STATES AS A FUNCTION OF FREQUENCY & ENERGY
C FOR ALL THE GIVEN TEMPERATURES. ALSO GIVEN IS A PLOT
C OF THE DENSITY OF STATES VS ENERGY. THE PARAMETERS IN
C THE PLOT ROUTINE MAY HAVE TO BE VARIED DEPENDING ON
C THE DOS VALUES. ALSO GIVEN ARE STATISTICS FOR A
C LEAST MEAN SQUARES ESTIMATE FOR THE LINE. THIS WOULD
C BE APPROPRIATE FOR AN EXPONENTIAL DISTRIBUTION OF
C STATES.
C
C
      INTEGER DATPT, DATNUM, S, J, COUNT, K
      REAL FREQ(10,30), PHASE(10,30), TVSIGM(10,30)
      REAL PIKT, KT, TEMP(10), SUM, TROC, ICALC(30)
      REAL ATEF,ENERGY(10,30), DEN(302), NRG(302)
      REAL LOGF, LOGI, W(5), TMP, SUMX, SUMY, SUMXY
      REAL SXX, SYY, SXY, R1, R2, A, B, SUMY2
      REAL TANPHI(30), WFREQ(10,30), IBUFF(4000), SUMX2
      SUMX=0.0
      SUMY=0.0
      SUMXY=0.0
      SUMX2=0.0
      SUMY2=0.0
```

```
      READ *,ATEF
      READ *, RUNS
C***  ATTEMPT TO ESCAPE FREQUENCY
C***  NUMBER OF DIFFERENT TEMPERATURES
      COUNT=1
      K=1
1     IF (COUNT .GT. RUNS) GO TO 7
11       READ *,TEMP(COUNT)
C***     READ AND DEFINE TEMPERATURE DEPENDENT
C***     VARIABLES
         TEMP(COUNT)=TEMP(COUNT)+273.23
         PIKT=2.71E-04*TEMP(COUNT)
         KT=8.62E-05*TEMP(COUNT)
         READ *,DATNUM
C***     READ NUMBER OF DATA PAIRS AT THIS TEMPERATURE
C***     AND THEN READ IN THE DATA
         READ *,(FREQ(COUNT,DATPT), PHASE(COUNT,DATPT),
     *           DATPT=1,DATNUM)
C***     CHANGE PHASE TO RADIANS, AND FREQ TO
C***     RADIANS/SECOND
         DATPT=1
2        IF (DATPT .GT. DATNUM) GO TO 18
            TANPHI(DATPT)=TAN(PHASE(COUNT,DATPT)/57.296)
            WFREQ(COUNT,DATPT)=
     *      6.28315*FREQ(COUNT,DATPT)
            ENERGY(COUNT,DATPT)=KT*ALOG(ATEF/WFREQ(COUNT,
     *                                     DATPT))
            DATPT=DATPT+1
            GO TO 2
C***     CALCULATE THE FREQUENCY DEPENDENCE OF THE DOS
18       TVSIGM(COUNT,1)=TANPHI(1)/PIKT
         J=2
3        IF(J .GT. DATNUM) GO TO 17
            S=2
            SUM=0
4           IF (S .GT. J) GO TO 16
               SUM=SUM+KT*ALOG(WFREQ(COUNT,S)/WFREQ(COUNT,S-1))
     *            *TVSIGM(COUNT,S-1)
               S=S+1
               GO TO 4
16          TVSIGM(COUNT,J)=(SUM+1)*TANPHI(J)/PIKT
            J=J+1
            GO TO 3
C***     CALCULATE THE THEORETICAL TRANSIENT
C***     PHOTOCURRENT MAGNITUDE
17       ICALC(1)=1.0
         TROC=SQRT((PIKT*TVSIGM(COUNT,1))**2+(PIKT*TVSIGM
     *           (COUNT,1)/TANPHI(1))**2)
         J=2
5        IF(J .GT. DATNUM) GO TO 15
            ICALC(J)=TROC/SQRT((PIKT*TVSIGM(COUNT,J))**2+
     *      (PIKT*TVSIGM(COUNT,J)/TANPHI(J))**2)
            J=J+1
            GO TO 5
```

```
C***      PRINT ALL THE RELEVANT DATA
15           TMP=TEMP(COUNT)-273.23
             PRINT 300,TMP, TEMP(COUNT), ATEF
          J=1
          PRINT 100
6         IF (J .GT. DATNUM) GO TO 19
             DEN(K)=ALOG10(TVSIGM(COUNT,J))
             LOGF=ALOG10(FREQ(COUNT,J))
             LOGI=ALOG10(ICALC(J))
             PRINT 200,FREQ(COUNT,J), PHASE(COUNT,J),
     *       ICALC(J),LOGI,LOGF, DEN(K), ENERGY(COUNT,J)
             NRG(K)=ENERGY(COUNT,J)
C***     CALCULATE STATISTICAL QUANTITIES
             SUMX=SUMX+NRG(K)
             SUMY=SUMY+DEN(K)
             SUMXY=SUMXY+NRG(K)*DEN(K)
             SUMX2=SUMX2+NRG(K)**2
             SUMY2=SUMY2+DEN(K)**2
             K=K+1
             J=J+1
             GO TO 6
19        COUNT=COUNT+1
          GO TO 1
7       PRINT 400
        SXX=SUMX2-SUMX**2/(K-1)
        SYY=SUMY2-SUMY**2/(K-1)
        SXY=SUMXY-SUMX*SUMY/(K-1)
C***    CALCULATE SLOPE
        A=((K-1)*SUMXY-SUMX*SUMY)/((K-1)*SUMX2-SUMX**2)
C***    CALCULATE Y INTERCEPT
        B=(SUMY*SUMX2-SUMX*SUMXY)/((K-1)*SUMX2-SUMX**2)
C***    CALCULATE CORRELATION COEFFICIENT
        R1=A*(SXX/SYY)**.5
        PRINT 800
        PRINT 500, A
        PRINT 600, B
        PRINT 700, R1
C***    FILL UP DATA ARRAYS WITH DUMMY CONSTANTS
8       IF (K .GT. 300) GO TO 20
           DEN(K) = 0.0
           NRG(K) = .3
           K=K+1
           GO TO 8
20      PRINT 400
C***    DEFINE PLOT CONSTANTS
        DEN(301)=0.0
        DEN(302)=1.0
        NRG(301)=0.3
        NRG(302)=0.05
C***    PLOT DATA
        CALL ROTATE(90)
        CALL AREA(10.75, 8.25)
        CALL PLOTS(IBUFF,4000)
        CALL PLOT(2.0, 2.0, -3)
```

```
      CALL AXIS(0.0, 0.0, 'ENERGY BELOW CB', -15, 8.0,
     *     0.0, .3, .05)
      CALL AXIS(0.0, 0.0, 'LOG(DENSITY)', 12, 4.0,
     *     90.0, 0.0, 1.0)
      CALL LINE(NRG, DEN, 300, 1, -1, 3)
      CALL PLOT(12.0, 0.0, 9999)
      STOP
100   FORMAT('-', 6X,'FREQUENCY',5X, 'PHASE',10X,
     *      'ICALC', 9X,'LOG(I)',4X
     *        'LOG(F)',3X,'LOG(DENS)',4X,'ENERGY')
200   FORMAT('0',6X,F7.2,6X,F5.1,5X,E14.4,5X,F6.3,
     *      5X,F5.3,5X.F6.3,5X,F7.4)
300   FORMAT('1',//9X,'TEMPERATURE= ',F6.2,' DEGREES
     *       CELCIUS',
     *      '   ,   ',F6.2,' DEGREES KELVIN',/,8X,
     *      ' ATTEMPT TO ESCAPE FREQUENCY = ',E12.4)
400   FORMAT('1')
500   FORMAT('0',10X,'SLOPE= ',E14.4)
600   FORMAT('0',10X,'Y INTERCEPT = ',E14.4)
700   FORMAT('0',10X,'CORRELATION COEFFICIENT =
     *       ',E14.4)
800   FORMAT('0',//5X,'STATISTICAL DATA USING LEAST
     *       MEAN SQUARES',/,
     *5X,'CURVE FITTING ALGORITHM:')
      END
//GO.FT05F001 DD *
//GO.FT22F001 DD SYSOUT=A
//GO.FT23F001 DD *
 &EPIC IMGDSP=-2,DPRESO=150,IOVRMX=300 &END
/*
//GO.FT24F001 DD
DSN=&&FT01F001,SPACE=(6144,300),UNIT=SYSDA,
//
DISP=(,PASS),DCB=(BLKSIZE=6144,RECFM=F,DSORG=DA,OPTCD=C)
//S2 EXEC XPLOT
//
```

REFERENCES

1. G. Aktas and Y. Skarlatos, J. Appl. Phys. 55, 3577(1984).
2. D. A. Anderson, G. Moddel, R. W. Collins and W. Paul, Sol. St. Comm. 31, 677(1979).
3. F. Boulitrop and D. J. Dunstan, Sol. St. Comm. 44, 841(1982).
4. R. H. Bube, Photoconductivity of Solids. Wiley, New York, 1960.
5. I. Chen, J. Appl. Phys. 47, 2988(1976).
6. M. H. Cohen, H. Fritzsche, and S. R. Ovshinsky, Phys. Rev. Lett. 22, 1065(1969).
7. M. H. Cohen, J. Non-Cryst. Sol. 4, 391(1970).
8. E. A. Davis and N. F. Mott, Phil. Mag. 22, 903(1970).
9. W. den Boer, J. de Physique 42, C4-451(1981).
10. W. Fuhs and M. Milleville, Phys. Stat. Sol. B98, K29(1980).
11. S. Furukawa, T. Kagawa, and N. Matsumoto, Sol. St. Comm. 44, 927(1982).
12. N. B. Goodman and H. Fritzsche, Phil. Mag. B42, 149(1980).
13. N. B. Goodman, H. Fritzche and H. Ozaki, J. Non-Cryst. Sol. 35 & 36, 599(1980),

14. M. Grünewald, K. Weber, W. Fuhs, and P. Thomas, J. de Physique 42, C4-523(1981).

15. T. V. Herak, R. D. McLeod, K. C. Kao, H. C. Card, H. Watanabe K. Katoh, M. Yasui, and Y. Shibata, J. Non-Cryst. Sol. 69, 39(1984).

16. H. Hirose, T. Suzuki and G. H. Dober, Appl. Phys. Lett. 34, 234(1979).

17. M. Hoheisel, R. Carrius and W. Fuhs, J. Non-Cryst. Sol. 63, 313(1984).

18. Y. Hoshino and K. Arishmo, J. Phys. E (GB) 16, 427(1983).

19. N. Ibaraki and H. Fritzsche, J. Non-Cryst Sol. 66, 231(1984)

20. N. M. Johnson and W. B. Jackson, J. Non-Cryst. Sol. 68, 147(1984).

21. D. Jousse, P. Viktorovitch, L. Vieux-Rochaz and A. Chenevas-Paule, J. Non-Cryst. Sol. 35&36, 767(1984).

22. E. Klier Phys. Stat. Sol. A67, K151(1981)

23. H. Krause, Phys. Stat. Sol. A 74, K151(1982).

24. H. Kurata, M. Mirose and Y. Osaka, Jap. J. Appl. Phys. 20, L811(1981).

25. M. A. Lampert and P. Mark, Current Injection in Solids. Academic Press, New York 1970.

26. K. Mackenzie, P. Le Comber, and W. Spear, Phil. Mag. B 46, 377(1982).

27. D. S. Misra, A. Kumar, and S. C. Agarwal, Phil. Mag. B49, L69(1984).

28. N. F. Mott and E. A. Davis, Electronic Processes in Non-Crystalline Materials. Clarendon, Oxford 1979.

29. N. F. Mott, Advan. Phys. 16, 49(1967).

30. N. F. Mott, J. Phys. C 13, 5433(1980).

31. A. R. Moore, Appl. Phys. Lett. 37, 327(1980).

32. P. Nagels in Amorphous Semiconductors. ed by M. H. Brodsky, SpringerVerlag, New York 1979.

33. S. Nešpurek and J. Sworakowski, J. Appl. Phys. 51, 2098(1980).

34. H. Oheda, J. Appl. Phys 52, 6693(1981).

35. H. Oheda, S. Yamasaki, T. Yoshida, A. Matsuda, H. Okushi, and K. Tanaka, Jap. J. Appl. Phys 21, L440(1982).

36. H. Okushi, Y. Tokomaru, S. Yamakashi, H. Oheda, and K. Tanaka, Phys. Rev. B25, 4313(1982).

37. J. I. Pankove (editor), Semiconductors and Semimetals. vol. 21, Academic Press, Florida, 1984.

38. M. J. Powell, Phil Mag B43, 93(1981).

39. B. Rauscher, H. Peleiderer and B. Bullemer, Phys. Stat. Sol. A78, 623(1983).

40. E. H. Rhodreick, Metal Semiconductor Contacts. Clarendon, Oxford, 1979.

41. W. van Roosbroeck, Phys. Rev. 101, 1713(1956).

42. A. Rose, Concepts in Photoconductivity and Allied Problems. Wiley, New York, 1963.

43. Y. Sano, K. Morigaki, I. Hirabayashi, Sol. St. Comm. 43, 439(1982).

44. J. Shah, Sol. St. Comm. 36, 199(1980).

45. J. Shah and A. Pinczuk, Sol. St. Comm. 42, 717(1982).

46. J. Singh and M. H. Cohen, J. Appl. Phys. 51, 413(1980).

47. I. Solomon, R. Benferhat, and H. Tran-Quoc, Phys. Rev. B30, 3422(1984).

48. W. E. Spear and P. G. LeComber, Phil. Mag. 33, 935(1976).

49. W. E. Spear and P. G. LeComber in The Physics of Hydrogenated Amorphous Silicon I. ed by J. D. Joannopoulos and G. Lucovsky, SpringerVerlag New York, 1984.

50. W. E. Spear and H. L. Steemers, J. Non-Cryst. Sol. 66, 163(1984).

51. D. L. Staebler and C. R. Wronski, Appl. Phys. Lett. 31, 292(1977).

52. R. A. Street, Adv. in Phys. 30, 593(1981).

53. R. A. Street, J. C. Knights and D. K. Biegleson, Phys. Rev. B18, 1880(1980).

54. M. J. Thompson in The Physics of Hydrogenated Amorphous Silicon I. ed by J. D. Joannopoulos and G. Lucovsky, SpringerVerlag, New York, 1984.

55. M. Tomozane, I. Hasegawa, M. Kawabe and Y. Wannichi, Jap. J. Appl. Phys. 21, L49(1982).

56. H.Watanabe, K. Katoh, and M. Yasui, Jap. J. Appl. Phys. 23, 1(1984).

57. H. Watanabe, K. Katoh and M. Yasui, Jap. J. App. Phys. 21, L341(1982).

58. R. L. Weisfield, J. Appl. Phys. 54, 6401(1983).

59. W. Y. Xu, Z. L. Sun, Z. P. Wang and D. L. Lee, J. de Phys. 42, C4 695(1981).

60. M. Yamaguchi, J. Non-Cryst. Sol. 59 & 60, 425(1982).